SINGULAR HYPERBOLIC STRUCTURES ON PSEUDO-ANOSOV MAPPING TORI

A DISSERTATION
SUBMITTED TO THE DEPARTMENT OF MATHEMATICS
AND THE COMMITTEE ON GRADUATE STUDIES
OF STANFORD UNIVERSITY
IN PARTIAL FULFILLMENT OF THE REQUIREMENTS
FOR THE DEGREE OF
DOCTOR OF PHILOSOPHY

Kenji Kozai

June 2013

Abstract

We study three-manifolds that are constructed as mapping tori of surfaces with pseudo-Anosov monodromy. Such three-manifolds are endowed with natural singular Sol structures coming from the stable and unstable foliations of the pseudo-Anosov homeomorphism. We use Danciger's half-pipe geometry [6] to extend results of Heusener, Porti, and Suarez [13] and Hodgson [15] to construct singular hyperbolic structures when the monodromy has orientable invariant foliations and its induced action on cohomology does not have 1 as an eigenvalue. We also discuss a combinatorial method for deforming the Sol structure to a singular hyperbolic structure using the veering triangulation construction of Agol [1] when the surface is a punctured torus.

Preface

As a result of Perelman's Geometrization Theorem, every 3-manifold decomposes into pieces so that each piece admits one of eight model geometries. Most 3-manifolds admit hyperbolic structures, and outstanding questions in the field mostly center around these manifolds. Having an effective method for describing the hyperbolic structure would help with understanding topology and geometry in dimension three. The recent resolution of the Virtual Fibering Conjecture also means that every closed, irreducible, atoroidal 3-manifold can be constructed, up to a finite cover, from a homeomorphism of a surface by taking the mapping torus for the homeomorphism [2]. Moreover, Thurston [29] showed that if the homeomorphism is pseudo-Anosov, then the resulting 3-manifold M_ϕ is hyperbolic. Thus, mapping tori with pseudo-Anosov monodromy play an important role in studying hyperbolic 3-manifolds. Pseudo-Anosov homeomorphisms are ubiquitous in low dimensional topology, so understanding this construction has potential impacts in other areas of the field.

However, Thurston's proof is non-constructive, so understanding the hyperbolic structure on the mapping torus requires other tools. There is a more natural geometry, Sol geometry, on the manifold coming from the pseudo-Anosov flow on the surface. Some work has been done to find a connection between the two geometries by Hodgson [15] and Heusener, Porti, and Suárez [13] in the punctured torus case. Yet, not much is known in the more general case of pseudo-Anosov homeomorphisms of hyperbolic surfaces. The question of understanding hyperbolic geometry from the pseudo-Anosov

homeomorphism motivates the research in this dissertation.

Another way to understand hyperbolic 3-manifolds when they have non-empty boundary is to construct them as a set of hyperbolic ideal tetrahedra that have been glued together along faces. Epstein and Penner [8] have shown that hyperbolic 3-manifolds admit a "nice" decomposition into ideal (hyperbolic) polyhedra, but the existence of an ideal triangulation is unknown. Agol [1] recently constructed a canonical triangulation of mapping tori of pseudo-Anosovs using an invariant train track. Initially, there was hope that the resulting veering triangulation could be realized geometrically, but a counter-example was recently found by Issa [19]. Nonetheless, the construction may still have applications to hyperbolic geometry. In this dissertation, we study some of the properties of veering triangulations and prove some partial results on nearly collapsed ideal triangulations.

Acknowledgment

I would like to thank my advisor, Steven Kerckhoff, for his guidance during my time at Stanford University. I am grateful for his incredible patience and understanding during this process, and his ideas and advice were invaluable to my research. His ability to convey his insights and geometric intuition were critical to my success. I was also fortunate to have Jeffrey Danciger as an academic brother. His willigness to share his experience and suggestions – as related to research and otherwise – are greatly appreciated.

I would also like to express my gratitude to Ronen Mukamel for his insights on flat structures and translation surfaces, and David Futer, Henry Segerman, and Craig Hodgson for discussions in Luminy on veering triangulations. I have also enjoyed mathematical conversations with Jason DeBlois, Thomas Church, and Maryam Mirzakhani during my time at Stanford.

The camaraderie amongst the graduates students at Stanford made my experience at Stanford more enjoyable. In particular, I would like to thank officemates Luis Diogo, Christopher Henderson, and Henry Adam, as well as the fellow students in my Ph.D. class. The encouragement and support from those in the Department of Mathematics, as well as from Emily Gu, Tom Lam, and Helen Shi, made this dissertation possible.

Contents

List of Figures

Chapter 1

Introduction

1.1 Sol structures on mapping tori

Suppose S is a surface with negative Euler characteristic and $\phi : S \to S$ is a pseudo-Anosov homeomorphism. The stable and unstable foliations of ϕ determine a singular Euclidean structure on S, with the leaves of the foliations acting as the coordinate directions. The invariant foliations of ϕ are expanded and contracted by the dilatation factor, λ, and its inverse λ^{-1} (see Chapter 3 for more on pseudo-Anosov maps). Let M_ϕ be the mapping torus of S,

$$M_\phi = S \times [0,1]/(x,0) \sim (\phi(x),1)$$

We can imagine a geometry on M_ϕ so that in the fiber $S \times 0$, we have the singular Euclidean structure on S, described above. On a fiber $S \times t$, we can expand and contract the foliations so that at $t = 1$, we have expanded by λ and contracted by λ^{-1}.

Sol geometry, one of the eight Thurston geometries and discussed in further detail in Section 2.4, also has this geometric structure. Thinking of Sol in coordinates

(x, y, z), at a plane $z = c$, the geometry on the plane is similar to that of Euclidean geometry. As we translate in the z direction, the y direction is expanded and the x direction is contracted. Thus, M_ϕ admits a natural singular Sol structure, with singular set Σ given by the orbits of the singular points of the Euclidean structure on S. The Sol structure on M_ϕ is closely related to the pseudo-Anosov map, and so it can be easily understood in terms of properties of ϕ and its invariant foliations. The motivation for this dissertation is to understand the hyperbolic metric from the more easily understood singular Sol structure.

1.2 Connections to hyperbolic structures

The hyperbolization theorem of Thurston [29] for pseudo-Anosov mapping tori states that M_ϕ admits a complete hyperbolic structure. Moreover, by Mostow-Prasad Rigidity, this hyperbolic structure is unique. However, if we allow incomplete structure on M_ϕ, it is possible to find a family of hyperbolic structures with cone singularities, and when the cone angles are small, the family is parametrized by the cone angles [16]. In other words, we can deform the hyperbolic structures by varying the cone angles.

In Chapter 4 we investigate the connection between the hyperbolic structure on M_ϕ and the singular Sol structure coming from the invariant foliations of ϕ. In the case where S is a punctured torus, Hodgson [15] and Heusener, Porti, and Suárez [13] find singular hyperbolic structures that collapse to a 2-dimensional or 1-dimensional. By rescaling this collapse, they are able to recover the Sol structure on M_ϕ. We generalize these results in Chapter 4 to show the following.

Theorem 4.5 . Let $\phi : S \to S$ be a pseudo-Anosov homeomorphism whose stable and unstable foliations, $\mathcal{F}^s$ and $\mathcal{F}^u$, are orientable and ϕ^* does not have 1 as an eigenvalue. Then, there exists a family of singular hyperbolic structures on M_ϕ, smooth on the complement of Σ, that degenerate to a transversely hyperbolic foliation.

The degeneration can be rescaled so that the path of rescaled structures limit to the singular Sol structure on M_ϕ, as projective structures.

Sol geometry contains transverse embedded hyperbolic planes. These hyperbolic planes can be seen as the upper half-plane model of $\mathbb{H}^2$ in Sol or as the "lower half-plane model" (i.e. the upper half-plane model flipped upside-down). In Section 4.1, we exploit that geometry to project the Sol structure on M_ϕ to one of the hyperbolic planes, which gives a transversely hyperbolic foliation of M_ϕ and a representation of $\pi_1(M_\phi)$ into the group of isometries of $\mathbb{H}^2$. A transversely hyperbolic foliation can be viewed as a collapse of the 3-dimensional hyperbolic structure to a 2-dimensional one.

We then show in Section 4.2 that the space of representations (modulo conjugation) is smooth at this representation when ϕ has orientable invariant foliations and ϕ^* does not have 1 as an eigenvalue, allowing us to deform the representation. A key ingredient is the use of half-pipe (HP) geometry from Danciger [6] and discussed in Section 2.6, as an intermediate. We use the above information to find a HP representation which limits to the Sol representation, and apply the Ehresmann-Thurston principle to show that the representations correspond to geometric structures in a neighborhood of Sol structure. This allows us to find a family of singular hyperbolic structures that collapse, and by rescaling the degeneration, we can recover the singular Sol structure. These three-dimensional geometries can all be viewed in terms of projective structures (Section 2.3 for hyperbolic geometry, Section 2.4 for Sol geometry, and Section 2.6 for HP), and the deformation occurs as a smooth family of projective structures that transition from hyperbolic to HP/Sol.

The structures obtained in this matter have cone angles roughly equal to the cone angles of the singular Euclidean metric on S. Up to first order, a weighted sum of the change in the cones angles is negative, as shown in Section 4.4. Since the singular Euclidean metric has cone angles at least 4π, this means that we can choose all of

the cone angles to be decreasing. The results in Chapter 4 are about infinitesimal deformations, so further work would be required to show that the cone angles can be decreased to 2π, yielding a smooth hyperbolic structure. A result of this manner would allow us to understand the hyperbolic structure on pseudo-Anosov mapping tori from the topological properties of the map.

1.3 Veering triangulations

Given a pseudo-Anosov mapping class $\phi : S \to S$, Agol [1] describes a way of triangulating the mapping torus M_ϕ using triangulations on the surface S dual to the maximal splitting sequence of an invariant train track τ. At each stage of the splitting sequence, the branches with maximal weight are split, and the dual of these splits correspond to diagonal exchanges on quadrilaterals, giving rise to flattened tetrahedra. A natural taut angle structure is given by assigning π angles to the diagonals of the flattened tetrahedra and dihedral angles of 0 to the other edges. An important property of this triangulation is that it is veering [1, Proposition 4.2], which can be viewed as a condition on how vertices of tetrahedra move in the singular Euclidean structure on S or as a purely combinatorial condition involving labeling edges [18].

Hodgson, Rubinstein, Segerman, and Tillman [18], and Futer and Guéritaud [10] prove the existence of angle structures on these flattened tetrahedra where all of the angles are strictly between 0 and π. Realizing the topological triangulation as a geometric one where ideal tetrahedra are glued together along faces involves finding shape parameters for the tetrahedra that satisfy the *edge consistency equations*. In Chapter 5, we study veering triangulations and their properties, finding real solutions to the edge consistency equations in Section 5.3.

Theorem 5.8 . The assignment of shape parameters to tetrahedra using the projection to $\mathbb{R} \subset \partial\mathbb{H}^2$ using the weights of the dual branch as the $\mathbb{R}$-lengths of the

edges gives a solution to the edge consistency equations where the π angles are at the topmost tetrahedra in each fan.

The real solutions to the edge consistency equations correspond to degenerate tetrahedra that have been collapsed onto a 2-dimensional hyperbolic plane, and the theorem also gives combinatorial control of the angle structure in the collapse. Danciger [6] proved Theorem 5.8 in the punctured torus case, and the methods in Section 5.3 generalize the result to all veering triangulations where the fiber can be any hyperbolic surface. From here, the desired outcome would be to deform the flattened tetrahedra to non-degenerate, positive volume tetrahedra, so that we have a legitimate 3-dimensional hyperbolic structure (possibly singular) on M_ϕ. We reprove these deformation results for the punctured torus case by using the combinatorics of the triangulation.

Theorem 5.13 . Let S be a punctured torus and $\phi : S \to S$ pseudo-Anosov. Then there exists a triangulation of $N_\phi = M_\phi \setminus \Sigma$ and degenerate (real) solutions to the edge consistency equations that can be deformed to a solution with non-degenerate, positive volume tetrahedra.

Theorem 5.13 is a new proof of the same result by Danciger [6] using the combinatorics of the veering triangulation. It involves translating inequalities about the space of deformations of the tetrahedra into directed edges on a related triangulation of the cusp tori. An induction argument can then be used to find directed cycles on the tori, which imply that the inequalities can only be satisfied by equality. Results of Choi [4] then imply that the solution in Theorem 5.8 can be deformed. The general case of a hyperbolic surface using the combinatorial techniques appears to be much harder, but an application to the minimal dilatation 4-strand braid can be seen in Section 5.7. As with Theorem 4.5, these results are infinitesimal, meaning we can deform the triangulation for some ϵ amount. Deforming all the way to the complete structure

would require additional analysis of the space of solutions to the edge consistency equations.

Chapter 2

Geometric Structures

2.1 (X, G) structures

Let X be a manifold and G be a group acting on X. We will study geometric structures on a manifold M through the framework of (X, G)-structures described by Ehresmann [7] and Thurston [27]. We think of X as the model space (such as $\mathbb{E}^n$ or $\mathbb{H}^n$) and G the group of isometries of X. The necessary definitions will be restated here, and further treatment of the material can be found in Thurston [27].

Definition 2.1. A (X, G) *structure* on a manifold M is a collection of charts $\{\psi_\alpha : U_\alpha \to X\}$, where the $\{U_\alpha\}$ are an open cover of M, such that the transition maps $\psi_\alpha \psi_\beta^{-1}$ are restrictions of elements $g_{\alpha\beta} \in G$.

Examples of (X, G) structures include $(\mathbb{H}^3, \mathrm{Isom}(\mathbb{H}^3))$-structures or hyperbolic structures using any of the models for hyperbolic structures discussed in Section 2.3, $(\mathrm{Sol}, \mathrm{Isom}(\mathrm{Sol}))$-structures using any of the models for Sol discussed in Section 2.4, or $(\mathrm{HP}, \mathrm{Isom}(\mathrm{HP}))$-structures using any of the models for HP geometry discussed in Section 2.6. When it is clear that $G = \mathrm{Isom}(X)$, we will sometimes omit the structure group and call it an X-structure.

We assume in general that G is analytic so that any element of G is determined by its restriction to any open subset of X. Let M be any (X, G)-manifold. Fix a coordinate chart $\psi_0 : U_0 \to X$, and let $\{U_0, U_1, U_2, \dots\}$ be an open cover of M with respective maps $\psi_i \to X$. Then there are transition maps γ_{ij} so that $\gamma_{ij} \circ \psi_i = \psi_j$ where each γ_{ij} is the restriction of an element $g_{ij} \in G$ on $\psi_i(U_i \cap U_j)$. In other words, γ_{ij} is determined by a locally constant map on $U_i \cap U_j$.

Let α be a path in M beginning in U_0. We can find an analytic continuation of ψ_0 along α as follows: for any component of $\alpha \cap U_i$, the analytic continuation of ψ_0 along α is of the form $\gamma_i \circ \psi_i$ for some γ_i which is the restriction of an element $g_i \in G$. Since ψ_0 can be analytically continued along every path in M, there is a global analytic continuation of ψ_0 defined on the universal cover of M into X. This map, denoted $D : \tilde{M} \to X$ is called the *developing map*.

D is unique up to composition with elements of G. For any covering transformation T_α of $\tilde{M}$, there exists an element $g_\alpha \in G$ such that $D \circ T_\alpha = g_\alpha \circ D$. It is easily checked that this map $\rho : \alpha \mapsto g_\alpha$ is a homomorphism, which is called the *holonomy* of M.

Definition 2.2. M is *complete* as a (X, G)-manifold if $D : \tilde{M} \to X$ is a covering map.

In the case where M is a complete (X, G)-manifold and X is simply connected, then the developing map D is a diffeomorphism. Identifying $\tilde{M} \cong X$ and $\Gamma = \rho(\pi_1(M))$, we can see that $M = X/\Gamma$.

2.2 Infinitesimal deformations

A smooth family of (X, G)-structures on a manifold M can be described by a family of developing maps $D_t : \tilde{M} \to X$ and corresponding holonomy representations $\rho_t : \pi_1(M) \to G$.

Definition 2.3. Two families of (X, G)-structures D_t and F_t such that $D_0 = F_0$ are equivalent if there exist a smooth family g_t of elements in G and a smooth family of diffeomorphisms ϕ_t defined on all but a small neighborhood of ∂M such that $D_t = g_t \circ F_t \circ \tilde{\phi}_t$ where $\tilde{\phi}_t$ is the lift of ϕ_t, $g_0 = 1$, and $\tilde{\phi}_0$ is the identity.

We can think of D_t and F_t as deformations of the same structure, D_0. Such a deformation D_t is trivial if D_0 is equivalent to the family of structures $F_t = D_0$. In this case, the holonomy representations also differ by conjugation by a smooth family g_t, i.e. $\rho_t = g_t \rho_0 g_t^{-1}$.

We will study deformations of geometric structures through their representations. A key fact about deformations and their representations is below (see Goldman [11] for a proof of Theorem 2.6).

Definition 2.4. The representation variety $\mathcal{R}(\pi_1(M), G)$ is the space of representations $\rho : \pi_1(M) \to G$ with the compact-open topology, up to conjugation.

Definition 2.5. The deformation variety $\mathcal{D}(M, (X, G))$ is the space of (X, G)- structures on M with the C^∞ topology on the developing maps, up to the equivalence defined above.

Theorem 2.6 (Thurston)**.** *The map hol* : $\mathcal{D}(M, (X, G)) \to \mathcal{R}(\pi_1(M), G)$ *taking an* (X, G) *structure to its holonomy representation is a local homeomorphism.*

Hence, instead of analyzing the developing maps, we can study deformations of geometric structures by analyzing $\mathcal{R}(\pi_1(M), G)$. Suppose we have a smooth family of representations $\rho_t : \pi_1(M) \to G$. We discuss how to study the infinitesimal change in ρ_t at ρ_0, as in Hodgson [15]. The derivative of the homomorphism condition $\rho_t(ab) = \rho_t(a)\rho_t(b)$ yields

$$\rho_t'(ab) = \rho_t'(a)\rho_t(b) + \rho_t(a)\rho_t'(b).$$

In order to normalize the derivative, we multiply on the right by $\rho_t(ab)^{-1}$, to translate back to the identity element.

$$\rho_t'(ab) = \rho_t'(a)\rho_t(a)^{-1} + \rho_t(a)\rho_t'(b)\rho_t(b)^{-1}\rho_t(a)^{-1}.$$

The second term, $\rho_t(a)\rho_t'(b)\rho_t(b)^{-1}\rho_t(a)^{-1}$ is defined to be $\mathrm{Ad}_{\rho_t(a)}(\rho_t'(b)\rho_t(b)^{-1})$.

Let the Lie algebra of G be denoted by $\mathfrak{g}$. Then a cocycle $c : \pi_1(M) \to \mathfrak{g}$ is the map $c(\gamma) = \rho'(\gamma)\rho_0(\gamma)^{-1}$, where ρ' is the derivative evaluated at $t = 0$. The map c satisfies the cocycle condition

$$c(ab) = c(a) + \mathrm{Ad}_{\rho_0(a)}c(b). \tag{2.1}$$

The group of all maps satisfying the cocycle condition in Equation 2.1 is denoted $Z^1(\pi_1(M), \mathfrak{g}_{\mathrm{Ad}_{\rho_0}})$. Differentiating the triviality condition for representations $\rho_t = g_t\rho_0 g_t^{-1}$ yields the coboundary condition

$$c(\gamma) = u - \mathrm{Ad}_{\rho_0(\gamma)}u \tag{2.2}$$

for some $u \in \mathfrak{g}$. Cocycles satisfying Equation 2.2 are denoted $B^1(\pi_1(M), \mathfrak{g}_{\mathrm{Ad}_{\rho_0}})$. We have the following theorem about deformations of representations.

Theorem 2.7. *If $\mathcal{R}(\pi_1(M), G)$ is smooth at ρ_0, then the cohomology group,*

$$H^1(\pi_1(M), \mathfrak{g}_{Ad_{\rho_0}}) = Z^1(\pi_1(M), \mathfrak{g}_{Ad_{\rho_0}})/B^1(\pi_1(M), \mathfrak{g}_{Ad_{\rho_0}}),$$

describes the tangent space to $\mathcal{R}(\pi_1(M), G)$ at ρ_0.

Hence, at an infinitesimal level, we can study the space of cocycles to determine deformations of a representation ρ_0.

2.3 Hyperbolic geometry

In this section, we will provide a brief overview of hyperbolic geometry as relevant to the rest of this dissertation. A more thorough treatment can be found in Thurston [27] or the expanded version edited by Levy [20]. The models we will use for 3-dimensional hyperbolic space are the upper half-space model, hyperboloid model, and projective model.

The upper half-space model for hyperbolic space is obtained by taking the half-space

$$\mathbb{H}^3 = \{(x_1, x_2, x_3) \in \mathbb{R}^3 : x_3 > 0\},$$

with the metric

$$ds^2 = \frac{dx_1^2 + dx_2^2 + dx_3^2}{x_3^2}.$$

The boundary of $\mathbb{H}^3$ is the one-point compactification of the plane $x_3 = 0$ along with the point at infinity (∞). The infinite geodesics in this model are half-circles meeting the boundary at right angles. By identifying points on the boundary $(x_1, x_2, 0)$ with $z = x_1 + x_2 i$, we can describe it as $\partial\mathbb{H}^3 = \mathbb{C}P^1$. The isometry group in this model is $\mathrm{Isom}(\mathbb{H}^3) \cong \mathrm{PSL}(2, \mathbb{C})$, the group of mobius transformations acting on the boundary, $\mathbb{C}P^1$. An element

$$\begin{bmatrix} a & b \\ c & c \end{bmatrix} \in \mathrm{PSL}(2, \mathbb{C})$$

represents the map $z \mapsto \frac{az+b}{cz+d}$ acting on $\mathbb{C}P^1$.

The hyperboloid model is described as a subspace of $\mathbb{R}^{3,1}$. Topologically, $\mathbb{R}^{3,1}$ is the space $\mathbb{R}^4$, but it is endowed with the Lorentzian metric $ds^2 = -dx_1^2 + dx_2^2 + dx_3^2 + dx_4^2$. Then, the induced metric on

$$\mathbb{H}^3 = \{\vec{x} = (x_1, x_2, x_3, x_4) \in \mathbb{R}^{3,1} : ||\vec{x}|| = -1\}/\{\pm I\}$$

is isometric to the hyperbolic metric. The isometry group of $\mathbb{H}^3$ in the hyperboloid model is the identity component $\mathrm{SO}^+(3,1)$ of $\mathrm{SO}(3,1)$. Notice that each point in the hyperboloid model (which really are two points in $\mathbb{R}^{3,1}$ identified under the quotient by $\pm I$) intersects exactly 1 line through the origin in $\mathbb{R}^{3,1}$. Hence, we can also identify the hyperboloid with a subset of $\mathbb{R}P^3$, given by

$$\mathbb{H}^3 = \{\vec{x} = [x_1, x_2, x_3, x_4] \in \mathbb{R}P^3 : ||\vec{x}|| < 0\}.$$

There is a method for taking an isometry of $\mathbb{H}^3$ from the upper half-space model (i.e. an element $A \in \mathrm{PSL}(2,\mathbb{C})$) to the corresponding isometry in the hyperboloid model. First, a point (x_1, x_2, x_3, x_4) from the hyperboloid model is identified with the matrix

$$P(x_1, x_2, x_3, x_4) = \begin{bmatrix} x_1 + x_2 & x_3 + ix_4 \\ x_3 - ix_4 & x_1 - x_2 \end{bmatrix}.$$

Then, A acts on the point (x_1, x_2, x_3, x_4) by

$$AP(x_1, x_2, x_3, x_4)A^*,$$

where A^* denotes the Hermitian transpose of A. Notice that this operation preserves $\det P = x_1^2 - x_2^2 - x_3^2 - x_4^2$, so it sends points of the hyperboloid in $\mathbb{R}^{3,1}$ to points of the hyperboloid. The corresponding isometry in the hyperboloid model is the element $A' \in \mathrm{SO}(3,1)$ so that

$$AP(x_1, x_2, x_3, x_4)A^* = P(A'(x_1, x_2, x_3, x_4)).$$

Notice that there are multiple copies of $\mathbb{H}^3$ lying inside $\mathbb{R}^4$. For each $s > 0$, we

can take a different hyperboloid

$$\mathbb{H}^3_s = \{\vec{x} = (x_1, x_2, x_3, x_4) : -x_1^2 + x_2^2 + x_3^2 + s^2 x_4^2 = -1\}/\{\pm I\},$$

and the subgroup G_s of $\mathrm{GL}(4, \mathbb{R})$ preserving the form

$$-x_1^2 + x_2^2 + x_3^2 + s^2 x_4^2,$$

to obtain a space isometric to $\mathbb{H}^3$. The isometry is given by the rescaling map

$$\mathfrak{r}_s = \begin{bmatrix} 1 & 0 & 0 & 0 \\ 0 & 1 & 0 & 0 \\ 0 & 0 & 1 & 0 \\ 0 & 0 & 0 & s^{-1} \end{bmatrix}.$$

Geometrically, we can think of the family of hyperboloids, $\mathbb{H}^3_s$, as flattening out to $\mathbb{H}^2 \times \mathbb{R}$ in $\mathbb{R}^4$. Taking the limit as $s \to 0$ yields half-pipe geometry, discussed in Section 2.6.

2.4 Sol geometry

One of the eight Thurston geometries in three dimensions, Sol geometry has a natural link to pseudo-Anosov diffeomorphisms on surfaces. Topogically, Sol is $\mathbb{R}^3$, endowed with the metric $ds^2 = e^{2z}dx^2 + e^{-2z}dy^2 + dz^2$ at the point (x, y, z). The isometries of Sol are described by maps of the form,

$$(x, y, z) \mapsto (e^{-c}x + a, e^{c}x + b, z + c).$$

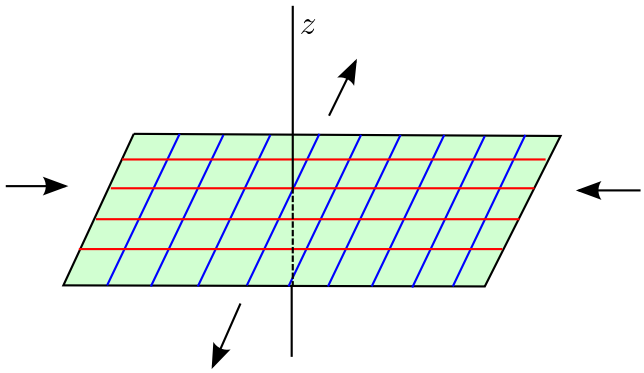

Figure 2.1: Translation in the z-direction contracts the x-direction and expands the y-direction in a slice of Sol.

In other words, translation in the z-direction contracts the x-direction by a factor of e^{-z} and expands the y-direction by a factor of e^{z}. On a fixed slice $z = z_0$, the isometries are given by translations.

Sol can also be embedded in $\mathbb{R}P^3$ by

$$(x, y, z) \mapsto \begin{pmatrix} \cosh z \\ \sinh z \\ e^z x \\ e^{-z} y \end{pmatrix}.$$

The isometry group of Sol in $\mathbb{R}P^3$ is the subgroup of PGL(4) consisting of elements of the form

$$\begin{bmatrix} \cosh z' & \sinh z' & 0 & 0 \\ \sinh z' & \cosh z' & 0 & 0 \\ x'e^{z'} & x'e^{z'} & 1 & 0 \\ y'e^{-z'} & -y'e^{-z'} & 0 & 1 \end{bmatrix},$$

where $\theta, x', y', z' \in \mathbb{R}$. A further treatment of Sol geometry can be found in Bonahon [3].

Note that by restricting Sol to certain two dimensional cross sections, we obtain hyperbolic planes inside Sol. For example, restricting to the yz-plane and $z > 0$ gives the upper half-plane model for $\mathbb{H}^2$, and restricting to the xz-plane with $z < 0$ is an inverted copy of the upper half-plane model. These hyperbolic planes within Sol will play an important role in Chapter 4. The idea will be to collapse the Sol structure onto a hyperbolic plane by projecting onto one of the leaves of $\mathcal{F}^u$. We will then think of this hyperbolic plane as living within $\mathbb{H}^3$, and we will regenerate the 3-dimensional hyperbolic structure from this collapsed structure.

2.5 Rescaling degenerations

In dimension three, Mostow-Prasad rigidity states that any fixed hyperbolic manifold has a unique complete hyperbolic structure, up to isometry. However, if we allow incomplete hyperbolic structures, then Thurston [27] showed that there is a deformation space of nearby (incomplete) hyperbolic structures. If the deformation is carried out far enough, the hyperbolic structure may degenerate, and the 3-manifold can collapse to a 2-dimensional or 1-dimensional manifold.

An analogous and simplified situation in 2-dimensional geometry can be observed for doubles of hyperbolic triangles. If we double the ideal hyperbolic triangle, we obtain a three-punctured sphere with cone angles of 0 at the three punctures. As the area of the triangles shrink, the sum of the cone angles approaches 2π. In the limit as the area approaches 0, the triangles degenerate to a point. If we rescale the triangles as they shrink, we obtain the double of a Euclidean triangle (Figure 2.2).

We can also see that we can continue to increase the cones angles, and we obtain the double of a spherical triangle. We can continue to deform the cone angles until the cone angle about each doubled vertex is 2π, giving the smooth sphere.

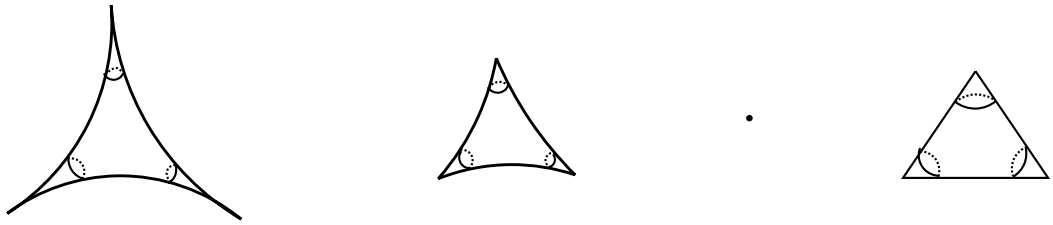

Figure 2.2: The double of a hyperbolic triangle collapses to a point as the sum of the cone angles at the vertices increases from 0 to 2π. Rescaling the collapse yields the double of a Euclidean triangle.

Thus, Euclidean geometry serves as the intermediate between hyperbolic and spherical geometry. Analogously, half-pipe geometry is the transition geometry between hyperbolic and AdS geometry in dimension three [6].

In the case that M is a punctured torus bundle, Hodgson [15] studied regenerations of singular hyperbolic metrics by taking a projection of the Sol structure onto one of its hyperbolic plane. Heusener, Porti, and Suárez [13] further showed that an appropriate rescaling of the degeneration yields the Sol metric on M_ϕ by using a more explicit construction. The reverse process of obtaining singular hyperbolic structures that degenerate so that a rescaling of the path of degenerating structures yields another geometric structure is called *regeneration*. We will be interested in regeneration of singular hyperbolic structures from the singular Sol metric on M_ϕ.

2.6 Half-pipe geometry

In his thesis, Danciger [6] studies degenerations of singular hyperbolic structures using the projective models. An appropriate rescaling of the degeneration yields half-pipe (HP) geometry, a transition geometry between hyperbolic geometry and anti-de Sitter (AdS) geometry.

Three-dimensional HP geometry, HP^n, topologically is $\mathbb{R}^n$. In terms of representations, it can be described as a rescaling of the collapse of the structure group from $\mathrm{SO}(3,1)$ to $\mathrm{SO}(2,1)$. Begin with a representation ρ_1 of $\pi_1(M)$ into $\mathrm{SO}(3,1)$, and describe the collapse the manifold in the x_4 coordinate by a family of representations ρ_t, so that we end with an representation ρ_0 into $\mathrm{SO}(2,1) \subset \mathrm{SO}(3,1)$ of matrices of the form

$$\begin{bmatrix} A \in \mathrm{SO}(2,1) & 0 \\ 0 & 1 \end{bmatrix}.$$

Conjugate the path of representations ρ_t degenerating in this matter by

$$\mathfrak{r}_t = \begin{bmatrix} 1 & 0 & 0 & 0 \\ 0 & 1 & 0 & 0 \\ 0 & 0 & 1 & 0 \\ 0 & 0 & 0 & \frac{1}{t} \end{bmatrix},$$

and take the limit as $t \to 0$. This will yield a representation ρ_{HP} whose image lies in the set of matrices of $\mathrm{O}(3,1)$ of the form

$$\begin{bmatrix} A \in \mathrm{SO}(2,1) & 0 \\ v & 1 \end{bmatrix} \tag{2.3}$$

where v is (the transpose of) a vector in $\mathbb{R}^3$. The vector v can be interpretted as an infinitesimal deformation of A into $\mathrm{SO}(3,1)$.

Another way to interpret the collapse is by using $\mathfrak{r}_t$. The map $\mathfrak{r}_t$ takes the standard copy of $\mathbb{H}^3$ inside $\mathbb{R}^{3,1}$ to the isometric copy $\mathbb{H}^3_t$. As we take the limit $t \to 0$, we obtain HP^3 as

$$\mathrm{HP}^3 = \lim_{t \to 0} \mathbb{H}^3_t = \{(x_1, x_2, x_3, x_4) : -x_1^2 + x_2^2 + x_3^2 = -1\}.$$

A concrete description of v can be found by generalizing the isomorphism $\mathrm{SO}(3,1) \cong$

$\mathrm{PSL}(2,\mathbb{C})$. Let κ_s be a non-zero element such that $\kappa_0^2 = -s^2$, and define an algebra $\mathcal{B}_s = \mathbb{R} + \mathbb{R}\kappa_s$ generated over $\mathbb{R}$ by 1 and κ_s. Furthermore, define a conjugation by

$$a + b\kappa_s \mapsto \overline{a + b\kappa_s} = a - b\kappa_s.$$

Then let A^* be the conjugate transpose of A.

We can define a map $P_s = \mathbb{H}^3_s \subset \mathbb{R}^{3,1} \to \mathrm{Herm}(2, \mathcal{B}_s)$ by

$$P_s(x_1, x_2, x_3, x_4) = \begin{bmatrix} x_1 + x_2 & x_3 + \kappa_s x_4 \\ x_3 - \kappa_s x_4 & x_1 - x_2 \end{bmatrix}$$

where $\mathrm{Herm}(2, \mathcal{B}_s)$ is the set of 2×2 matrices with entries in $\mathcal{B}_s$ such that $A = A^*$. Then define the map $\mathrm{PSL}(2, \mathcal{B}_s) \to G_s$ by $A \mapsto A'$ where A' is the matrix that satisfies

$$AP_s(x_1, x_2, x_3, x_4)A^* = P(A'(x_1, x_2, x_3, x_4)).$$

When $s = 1$, this is the usual isometry from $\mathrm{PSL}(2,\mathbb{C})$ to $\mathrm{SO}(3,1)$. Danciger proves the following:

Theorem 2.8 (Danciger [6], Propositions 25, 28)**.** *For $s > 0$, the map $PSL(2, \mathcal{B}_s) \to G_s$ is an isomorphism. When $s = 0$, the map $PSL(2, \mathcal{B}_0) \to G_0$ is an isomorphism onto the group of HP matrices.*

Moreover, in the case $s = 0$, we obtain a geometric interpretation for the vector v in Equation 2.3. If we have a matrix in $\mathrm{PSL}(2, \mathcal{B}_s)$, we can write it as $A + B\kappa_0$, where A is symmetric and B is skew-symmetric. Similarly, we can write $P_0(x_1, x_2, x_3, x_4) =$

$X + Y\kappa_0$ where

$$X = \begin{bmatrix} x_1 + x_2 & x_3 \\ x_3 & x_1 - x_2 \end{bmatrix}$$
$$Y = \begin{bmatrix} 0 & x_4 \\ -x_4 & 0 \end{bmatrix}.$$

Then $(A + B\kappa_0)(X + Y\kappa_0)(A + B\kappa_0)^* = AXA^T + (BXA^T - AXB^T + AYA^T)\kappa_0$. In the map $\mathrm{PSL}(2, \mathcal{B}_0) \to G_0$, the symmetric part AXA^T gives the first three rows of the HP matrix, and the skew-symmetric part $(BXA^T - AXB^T + AYA^T)$ gives the bottom row of the HP matrix.

Furthermore, we can compute that

$$\det(A + B\sigma) = \det A + \mathrm{tr}BA^{-1}\kappa_0.$$

Hence, if $A + B\kappa_0 \in \mathrm{PSL}(2, \mathcal{B}_0)$, then $A \in \mathrm{PSL}(2, \mathbb{R})$ and $\mathrm{tr}BA^{-1} = 0$, so that B is in $\mathfrak{sl}(2, \mathbb{R})A$. Hence, in (x_1, x_2, x_3, x_4) coordinates, the symmetric part is the usual map $\mathrm{PSL}(2, \mathbb{R}) \to \mathrm{SO}(2, 1)$, and the bottom row comes from the skew-symmetric part. The vector v in the HP matrix of Equation 2.3 is a tangent vector to the $\mathrm{SO}(2, 1)$ representation of the collapsed structure.

The key result about HP structures is that we can recover hyperbolic structures from them.

Theorem 2.9 (Danciger [6], Theorem 5)**.** *Let (M, Σ) be a closed HP^3 manifold with infinitesimal cone singularity of infinitesimal angle $-\omega$ along Σ and suppose that $\mathcal{R}(\pi_1(M \setminus \Sigma), SL(2, \mathbb{R}))$ is smooth at ρ_0, where ρ_0 is the $SO(2, 1)$ part of the representation. Then, there exist singular geometric structures on (M, Σ) parametrized by $t \in (-\delta, \delta)$ which are:*

1. *hyperbolic cone structures with cone angle* $2\pi - \omega t$ *for* $t > 0$,

2. *AdS structures with a tachyon mass* $-\omega t$ *for* $t < 0$.

Thus, if we can find an HP structure for M_ϕ, then we can deform it to nearby hyperbolic and AdS structures.

Chapter 3

Pseudo-Anosovs and surfaces

3.1 Pseudo-Anosov homeomorphisms

Let S be a surface with negative Euler characteristic and genus g.

Definition 3.1. The *mapping class group* of S, denoted $\mathrm{Mod}(S)$, is

$$\mathrm{Mod}(S) = \mathrm{Homeo}^+(S)/\mathrm{Homeo}_0(S),$$

where $\mathrm{Homeo}^+(S)$ is the set of orientation-preserving self-homeomorphisms of S, and $\mathrm{Homeo}_0(S)$ is the identity component.

Definition 3.2. A mapping class $f \in \mathrm{Mod}(S)$ is *pseudo-Anosov* if there exists a representative homeomorphism $\phi : S \to S$ with transverse (singular) measured foliations $(\mathcal{F}^u, \mu_u)$ and $(\mathcal{F}^s, \mu_s)$ on S and a number $\lambda > 1$ such that

$$\phi \cdot (\mathcal{F}^u, \mu_u) = (\mathcal{F}^u, \lambda\mu_u)$$
$$\phi \cdot (\mathcal{F}^s, \mu_s) = (\mathcal{F}^s, \lambda^{-1}\mu_s).$$

The measured foliations $(\mathcal{F}^u, \mu_u)$ and $(\mathcal{F}^s, \mu_s)$ are called the *unstable foliation* and

stable foliation, and λ is called the *dilatation factor* of f.

In an abuse of notation, whenever convenient, the distinction between a pseudo-Anosov mapping class f and a representative homeomorphism ϕ will be ignored, and both will be referred to as ϕ. By the Nielsen-Thurston classification [28], a mapping class $f \in \mathrm{Mod}(S)$ is finite order, reducible (meaning that it fixes a finite set of isotopy classes of simple closed curves), or pseudo-Anosov. In other words, another characterization is that a mapping class ϕ is pseudo-Anosov if and only if no power of ϕ fixes a simple closed curve, up to isotopy. A geometric interpretation of the stable and unstable foliations is that if we take a simple closed curve γ, then $\phi^n(\gamma)$ limits to $\mathcal{F}^u$ while $\phi^{-n}(\gamma)$ limits to $\mathcal{F}^s$.

The invariant foliations, $\mathcal{F}^u$ and $\mathcal{F}^s$, have a finite number of singularities. Otherwise, the invariant foliations would define a Euclidean metric on S, which is not possible under the assumption that S has negative Euler characteristic. We will denote the singularities by $\sigma = \{s_1, s_2, \ldots, s_n\}$. The homeomorphism ϕ is a diffeomorphism away from σ, and it is not smooth at the singularities. The measure, μ_u, is a measure on arcs transverse to $\mathcal{F}^u$, and it is invariant under isotopies that fix or translate the endpoints along leaves of $\mathcal{F}^u$.

We can encode an invariant lamination in a combinatorial object called a *train track*. A train track is a trivalent, C^1 graph on S, whose vertices are called *switches* and edges are called *branches*. A measured train track (τ, m_τ) is an assignment of numbers to the the branches so that the three branches that are coincident at a switch satisfy a switch condition. The branches can be thought of in the following way: in a neighborhood away from a singularity of $\mathcal{F}^{u/s}$, we have leaves of $\mathcal{F}^{u/s}$ which are parallel. Collapsing the parallel leaves onto a single leaf, we obtain an edge, which corresponds to a branch. The measure on the edge is the measure of an arc transverse to the leaves which were collapsed onto the branch, as in Figure 3.1. Notice that the choice of collapsing the leaves of the foliation onto these three branches have created a

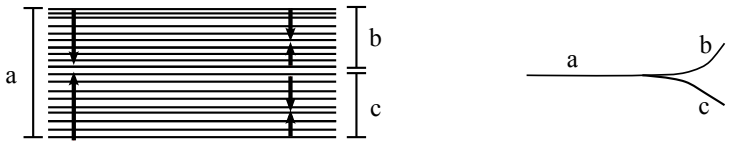

Figure 3.1: Left: A foliation with transverse measure. Right: The train track resulting from collapsing the indicated leaves.

switch, and the switch condition $a = b + c$ comes from the additivity of the transverse measure.

3.2 Pseudo-Anosov mapping tori

We can also form a 3-manifold from ϕ by taking the mapping torus $M_\phi = S \times [0,1]/(x,0) \sim (\phi(x),1)$. M_ϕ is a surface bundle over S^1. Thurston [29] showed that M_ϕ is hyperbolic if and only if ϕ is pseudo-Anosov. In the case where S has punctures, we can fill in a puncture by adding a point. If the foliation cannot be extended smoothly to the point, then the filled in puncture becomes a new singularity of the foliations. Thus, for the remainder of this disseration, we will only consider S to be a closed surface with genus $g > 1$ for notational simplicity, but the results will extend to the more general case of punctured surfaces with negative Euler characteristic.

The invariant foliations along with their transverse measures define a singular Euclidean metric on S. This is analogous to how $\mathbb{R}^2$ is foliated by the lines $x =$ constant and $y =$ constant. Moreover, since the pseudo-Anosov scales the foliations by λ and λ^{-1}, the pseudo-Anosov dynamics on the foliations acts in the same way as a Sol isometry translating by $\log \lambda$ in the z-direction. More specifically, we can define a pseudo-Anosov flow so that at time t, the foliations $\mathcal{F}^u$ and $\mathcal{F}^s$ are scaled by e^t and

e^{-t}. The mapping torus M_ϕ can be thought of as the set of points

$$\{(x,t) : x \in S, t \in [0, \log \lambda]\}$$

with the relation $(x,0) \sim (\phi(x), \log \lambda)$. The pseudo-Anosov flow on the surface fiber acts as a Sol isometry on the manifold, so we can put a singular Sol structure on M_ϕ, where the singularities Σ are fibers of the singularities σ.

3.3 Intersection symplectic form

For a closed surface S, there is a symplectic action of $\mathrm{Mod}(S)$ on the first homology, $H_1(S) = H_1(S, \mathbb{Z})$. Much of the discussion in this section follows Farb and Margalit [9].

Let $\{x_1, x_2, \ldots, x_g, y_1, y_2, \ldots, y_g\}$ be a basis for $\mathbb{R}^{2g}$. Let ω be the 2-form defined by

$$\omega = \sum_{i=1}^{g} dx_i \wedge dy_i.$$

The form ω is an alternating, nondegenerate bilinear form on $\mathbb{R}^{2g}$. Given two vectors $\vec{v} = (v_1, v_2, \ldots, v_g, w_1, w_2, \ldots, w_g)$ and $\vec{v'} = (v'_1, v'_2, \ldots, v'_g, w'_1, w'_2, \ldots, w'_g)$, we can compute

$$\omega(\vec{v}, \vec{v'}) = \sum_{i=1}^{g} v_i w'_i - v'_i w_i.$$

A vector space isomorphic to $\mathbb{R}^{2g}$ with such a form ω is a *symplectic vector space*. The symplectic group $\mathrm{Sp}(2g, \mathbb{R})$ is the subset of $2g \times 2g$ real matrices, $M(2g, \mathbb{R})$, that preserve ω,

$$\mathrm{Sp}(2g, \mathbb{R}) = \{A \in M(2g, \mathbb{R}) : A^* \omega = \omega\}.$$

The 2-form ω has the following properties:

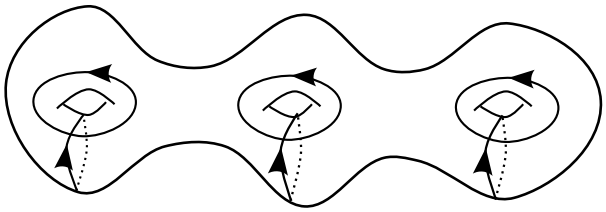

Figure 3.2: A symplectic basis for $H_1(S, \mathbb{R})$ with the algebraic intersection form.

1. $\omega(\vec{v}, \vec{v}') = -\omega(\vec{v}', \vec{v})$ (skew-symmetric),

2. $\omega(\vec{v}, \vec{v}) = 0$ (totally isotropic),

3. if $\omega(\vec{v}, \vec{v}') = 0$ for all $\vec{v}' \in \mathbb{R}^{2g}$, then $\vec{v} = 0$ (non-degenerate).

For homology classes $a, b \in H_1(S)$, the algebraic intersection number defines a map $i : H_1(S) \otimes H_1(S) \to \mathbb{Z}$. The map can be extended linearly to $H_1(S, \mathbb{R})$ to obtain a map

$$\hat{i} : H_1(S, \mathbb{R}) \otimes H_1(S, \mathbb{R}) \to \mathbb{R}.$$

It can be shown that $\hat{i}$ is a symplectic form on $H_1(S, \mathbb{R})$, acting on its dual $H^1(S, \mathbb{R})$. In particular, using the basis $\alpha_1, \alpha_2, \ldots, \alpha_g, \beta_1, \beta_2, \ldots, \beta_g$ as in Figure 3.2, the form $\hat{i}$ is the standard symplectic form, ω.

Consider a mapping class $\phi \in \mathrm{Mod}(S)$. Notice that ϕ_* preserves the algebraic intersection number $i(\cdot, \cdot)$, and moreover, it takes integral homology classes to integral homology classes. Hence,

$$\phi_* \in \mathrm{Sp}(2g, \mathbb{Z}) = \mathrm{Sp}(2g, \mathbb{R}) \cap \mathrm{GL}(2g, \mathbb{Z}).$$

The symplectic nature of $\mathrm{Mod}(S)$ will be exploited in Chapter 4, as $\mathcal{F}^{u/s}$ can be thought of as eigenvectors for ϕ^*.

Chapter 4

Regenerating hyperbolic structures

4.1 Representations from the invariant foliations

Let $\phi : S \to S$ be a pseudo-Anosov homeomorphism with orientable invariant foliations $\mathcal{F}^s, \mathcal{F}^u$ with singular set $\sigma = \{s_0, s_1, \ldots, s_n\}$ and transverse measures μ_s and μ_u. The orientability assumption gives us some control over the eigenvalues of $\phi^* : H^1(S) \to H^1(S)$.

Lemma 4.1 (McMullen [22], Theorem 5.3)**.** *Let ϕ be a pseudo-Anosov homeomorphism with dilatation factor λ. Suppose also that ϕ has orientable unstable and stable foliations, $\mathcal{F}^u$ and $\mathcal{F}^s$. Then λ and λ^{-1} are simple eigenvalues of ϕ^*.*

Proof. Let $\omega \in H^1(S)$ be any cohomology class dual to a simple closed curve γ. Since ϕ is pseudo-Anosov, $\phi^n(\gamma)$ limits to the unstable foliation. In particular,

$$\frac{(\phi^n)^*\omega}{\lambda^n} \to c\mathcal{F}^u$$

for some $c \neq 0$. Since the classes ω dual to simple closed curves span $H^1(S)$, λ is an eigenvalue of ϕ^*. It also follows that λ must be a simple eigenvalue by considering the Jordan canonical form. □

Note that in addition to λ and λ^{-1} being simple eigenvalues, we also have that the corresponding eigenvectors come from the measures $\mathcal{F}^u$ and $\mathcal{F}^s$. In particular, if we take $\gamma_1, \gamma_2, \ldots, \gamma_{2g}$ to be a basis for $H_1(S)$, then the eigenvector $\vec{e}_\lambda$ is given by

$$\vec{e}_\lambda = \begin{pmatrix} \mu_u(\gamma_1) \\ \mu_u(\gamma_2) \\ \vdots \\ \mu_u(\gamma_{2g} \end{pmatrix},$$

whereas the eigenvector corresponding to λ^{-1} is given by

$$\vec{e}_{\lambda^{-1}} = \begin{pmatrix} \mu_s(\gamma_1) \\ \mu_s(\gamma_2) \\ \vdots \\ \mu_s(\gamma_{2g}) \end{pmatrix}.$$

Let $\delta_1, \delta_2, \ldots, \delta_n$ be the generators of $\pi_1(S \setminus \sigma)$ coming from the punctures. We can think of the product $\delta_1\delta_2 \cdots \delta_n$ as the boundary ∂D of a disk D with all of the punctures in the interior of D.

Choose generators $\alpha_1, \alpha_2, \ldots, \alpha_g$ and $\beta_1, \beta_2, \ldots, \beta_g$ of $\pi_1(S)$ such that for each i, (a representative of) α_i and β_i do not intersect ∂D for $i = 1, \ldots, g$. The algebraic intersection number on oriented curves is a symplectic form on $H^1(S)$, and we also choose α_i and β_i so that they are a standard symplectic basis for this form. We will also refer to these curves as $\gamma_i = \alpha_i$, $\gamma_{g+i} = \beta_i$, $\gamma_{2g+j} = \delta_j$. When convenient, we will use α_i, β_i, and δ_j to refer to their respective homology classes.

On the dual generators $\alpha_i^*, \beta_i^*, \delta_j^*$ of $H^1(S \setminus \sigma)$, we have that ϕ^* has a block diagonal action: the first block corresponding to the action on the closed surface S, and the second block a permutation of the generators $\delta_1^*, \ldots, \delta_n^*$ coming from the punctures.

Strictly speaking, this matrix is a square matrix with dimensions one greater than the dimension of $H^1(S \setminus \sigma)$. There is one redundancy in the generators by the relation $\sum_{j=1}^{n} \delta_j = 0$ in homology. However, using the additional generator from the punctures makes the lower right block for ϕ^* easier to understand. When discussing $H^1(S \setminus \sigma)$ (or ϕ^*) in this section, it will mean $H^1(S \setminus \sigma)$ with this additional generator (resp. the action on $H^1(S \setminus \sigma)$ with the additional generator).

Using the generators for $\pi(S)$, we can describe $\Gamma = \pi_1(N = M_\phi \setminus \Sigma)$ by the following presentation.

$$\Gamma = \left\langle \{\alpha_i\}, \{\beta_i\}, \{\delta_j\}, \tau \;\middle|\; \begin{array}{c} \tau\alpha_i\tau^{-1} = \phi(\alpha_i), \tau\beta_i\tau^{-1} = \phi(\beta_i), \\ \tau\delta_j\tau^{-1} = w_j\delta_{k_j}w_j^{-1}, \Pi_{i=1}^{g}[\alpha_i, \beta_i] = \Pi_{j=1}^{n}\delta_j \end{array} \right\rangle,$$

where w_j are words in the α_is and β_is.

We start with a metabelian representation $\rho_0 : \Gamma \to \mathrm{PSL}(2, \mathbb{R})$ with

$$\rho_0(\gamma_i) = \begin{bmatrix} 1 & a_i = \mu_u(\gamma_i) \\ 0 & 1 \end{bmatrix},$$

where a_i is the signed length of γ_i in $\mathcal{F}^u$. Note that $a_i = 0$ for $2g < i \leq n$. We also set

$$\rho_0(\tau) = \begin{bmatrix} \sqrt{\lambda} & 0 \\ 0 & \sqrt{\lambda}^{-1} \end{bmatrix},$$

where τ is the generator in the S^1 direction of M_ϕ, and λ is the pseudo-Anosov dilatation factor of ϕ. There is a singular Sol structure on M_ϕ coming from the pseudo-Anosov action on $\mathcal{F}^u$ and $\mathcal{F}^s$, where $\mathcal{F}^u$ and $\mathcal{F}^s$ provide a singular flat (Euclidean) structure on the fibers of M_ϕ. We can think of the metabelian representation as a projection of the singular Sol structure onto a leaf of $\mathcal{F}^s$, which lies inside of Sol as a

hyperbolic plane. Such a projection yields a *transversely hyperbolic foliation* – locally, M_ϕ can be viewed as an open subset of $\mathbb{H}^2 \times \mathbb{R}$, and the pseudometric is given by the metric on the $\mathbb{H}^2$ factor and ignoring the second factor.

4.2 Smoothness of the representation variety

The goal is to deform ρ_0 to a representation into $\mathrm{PSL}(2,\mathbb{C})$, and to realize the representation as the holonomy representation of a $(\mathbb{H}^3, \mathrm{PSL}(2,\mathbb{C}))$-structure on N. We consider $\rho_0 \in \mathcal{R}(\pi_1(N), \mathrm{PSL}(2,\mathbb{R}))$ as a point in the representation variety of representations modulo conjugation. We associate to the tangent space of $\mathcal{R}(\pi_1(N), \mathrm{PSL}(2,\mathbb{R}))$ at ρ_0 with the cohomology group $H^1(\pi_1(N), \mathfrak{sl}(2,\mathbb{R})_{\mathrm{Ad}_{\rho_0}})$. We wish to find a twisted cocycle $c \in H^1(\pi_1(N), \mathfrak{sl}(2,\mathbb{R})_{\mathrm{Ad}_{\rho_0}})$. As in Heusener-Porti-Suárez [14], c is determined by its values on $\gamma_1, \ldots, \gamma_{2g+n}$, and τ, which we denote by

$$c(\gamma_i) = \begin{bmatrix} y_i & x_i \\ z_i & -y_i \end{bmatrix}$$

and, up to conjugation,

$$c(\tau) = \begin{bmatrix} y_0 & 0 \\ 0 & -y_0 \end{bmatrix}.$$

We first begin by computing the dimension of the space of such cocyles. A standard Poincare duality argument [24, 14, 17] gives that the map

$$H^1(\pi_1(N), \mathfrak{sl}(2,\mathbb{R})_{\mathrm{Ad}_\rho}) \to H^1(\pi_1(\partial N), \mathfrak{sl}(2,\mathbb{R})_{\mathrm{Ad}_\rho})$$

has half-dimensional image. Another standard argument then shows that for a torus T, $\dim H^1(\pi_1(T), \mathfrak{sl}(2,\mathbb{R})_{\mathrm{Ad}_\rho}) = 2$ as long as $\rho(\pi_1(T))$ contains a hyperbolic element [24]. Combined, we get the following result.

Lemma 4.2. $\dim H^1(\pi_1(N), \mathfrak{sl}(2,\mathbb{R})_{Ad_\rho}) \geq m$ *for any* ρ *near* ρ_0*, where* m *is the number of components of the boundary of* N*.*

Proof. For each (torus) boundary component of N, we have that $\rho_0(m) = I$ and $\rho_0(l)$ is a hyperbolic element by construction. Then all nearby ρ also contain hyperbolic elements. The previous remarks show that

$$\dim H^1(\pi_1(\partial N), \mathfrak{sl}(2,\mathbb{R})_{\mathrm{Ad}_\rho}) = 2m$$

for any ρ near ρ_0, and therefore

$$\dim H^1(\pi_1(N), \mathfrak{sl}(2,\mathbb{R})_{\mathrm{Ad}_\rho}) \geq m.$$

□

Hence the representation variety $\mathcal{R}(\pi_1(N), \mathrm{PSL}(2,\mathbb{R}))$ is smooth at ρ_0 as long as $\dim H^1(\Gamma, \mathfrak{sl}(2,\mathbb{R})_{\mathrm{Ad}_{\rho_0}}) = m$, and given an element $c \in H^1(\Gamma, \mathfrak{sl}(2,\mathbb{R})_{\mathrm{Ad}_{\rho_0}})$, we can deform ρ_0 in the direction of c.

Theorem 4.3. *Let* ϕ *be pseudo-Anosov with stable and unstable foliations which are orientable. Suppose also that* $\phi^* : H^1(S) \to H^1(S)$ *does not have 1 as an eigenvalue. Then* $\dim H^1(\Gamma, \mathfrak{sl}(2,\mathbb{R})_{Ad_{\rho_0}}) = m$ *where* m *is the number of components of the boundary of* N*.*

Proof. From the relations $c(\phi(\alpha_i)) - c(\tau\alpha_i\tau^{-1}) = 0$, $c(\phi(\beta_i)) - c(\tau\beta_i\tau^{-1}) = 0$, and $c(w_j\delta_{k_j}w_j^{-1}) - c(\tau\delta_j\tau^{-1}) = 0$, we find a $3(2g+n) \times 3(2g+n) + 1$ matrix R such that

$$R\vec{v} = 0,$$

where

$$\vec{v} = \begin{pmatrix} x_1 \\ \vdots \\ x_{2g+n} \\ y_0 \\ y_1 \\ \vdots \\ y_{2g+n} \\ z_1 \\ \vdots \\ z_{2g+n} \end{pmatrix}$$

is a vector describing c. Each relation can be represented by three rows in R. For example, we can calculate

$$\begin{aligned} c(\tau\alpha_i\tau^{-1}) &= c(\tau) + \mathrm{Ad}_{\rho_0}(\tau)\cdot c(\alpha_i) - \mathrm{Ad}_{\rho_0}(\tau\alpha_i\tau^{-1})\cdot c(\tau) \\ &= \begin{bmatrix} y_0 & 0 \\ 0 & -y_0 \end{bmatrix} + \begin{bmatrix} y_i & \lambda x_i \\ \lambda^{-1} z_i & -y_i \end{bmatrix} - \begin{bmatrix} y_0 & -2\lambda a_i y_0 \\ 0 & -y_0 \end{bmatrix}, \end{aligned}$$

and, expressing $\phi(\alpha_i)$ as a product $\gamma_{i_1}\gamma_{i_2}\cdots\gamma_{i_m}$, we can find

$$\begin{aligned} c(\phi(\alpha_i)) = \;& c(\gamma_{i_1}\gamma_{i_2}\cdots\gamma_{i_m}) \\ =\;& c(\gamma_{i_1}) + \mathrm{Ad}_{\rho_0}(\gamma_{i_1})\cdot c(\gamma_{i_2}) + \cdots + \mathrm{Ad}_{\rho_0}(\gamma_{i_1}\gamma_{i_2}\cdots\gamma_{i_{m-1}})\cdot c(\gamma_{i_m}) \\ =\;& \begin{bmatrix} y_{i_1} & x_{i_1} \\ z_{i_1} & -y_{i_1} \end{bmatrix} + \begin{bmatrix} y_{i_2} + a_{i_1} z_{i_2} & x_{i_2} - 2a_{i_1} y_{i_2} - a_{i_1}^2 z_{i_2} \\ z_{i_2} & -y_{i_2} - a_{i_1} z_{i_2} \end{bmatrix} \\ &+ \cdots + \begin{bmatrix} y_{i_m} + \sum_{l=1}^{m-1} a_{i_l} z_{i_m} & x_{i_m} - 2\sum_{l=1}^{m-1} a_{i_l} y_{i_m} - (\sum_{l=1}^{m-1} a_{i_l})^2 z_{i_m} \\ z_{i_m} & -y_{i_m} - \sum_{l=1}^{m-1} a_{i_l} z_{i_m} \end{bmatrix}. \end{aligned}$$

Then, we can rewrite the relation $c(\phi(\alpha_i)) - c(\tau\alpha_i\tau^{-1}) = 0$ as

$$\begin{bmatrix} 1 & 0 & 0 \\ 0 & 1 & 0 \\ 0 & 0 & 1 \end{bmatrix} \begin{pmatrix} x_{i_1} \\ y_{i_1} \\ z_{i_1} \end{pmatrix} + \begin{bmatrix} 1 & -2a_{i_1} & -a_{i_1}^2 \\ 0 & 1 & a_{i_1} \\ 0 & 0 & 1 \end{bmatrix} \begin{pmatrix} x_{i_2} \\ y_{i_2} \\ z_{i_2} \end{pmatrix}$$
$$+ \cdots + \begin{bmatrix} 1 & -2\sum_{l=1}^{m-1} a_{i_l} & -(\sum_{l=1}^{m-1} a_{i_l})^2 \\ 0 & 1 & \sum_{l=1}^{m-1} a_{i_l} \\ 0 & 0 & 1 \end{bmatrix} \begin{pmatrix} x_{i_m} \\ y_{i_m} \\ z_{i_m} \end{pmatrix}$$
$$- \begin{bmatrix} \lambda & 0 & 0 \\ 0 & 1 & 0 \\ 0 & 0 & \lambda^{-1} \end{bmatrix} \begin{pmatrix} x_i \\ y_i \\ z_i \end{pmatrix} - 2\lambda a_i \begin{pmatrix} y_0 \\ 0 \\ 0 \end{pmatrix} = 0$$

As in Heusener-Port-Suárez [14], we can let each row of R represent one relation of the above form, so that c can be described by a vector $\vec{v}$ such that $R\vec{v} = 0$. Then R decomposes into blocks

$$R = \left[\begin{array}{ccc|c|c|c} & & & -2\lambda a_1 & & \\ & \bar{\phi}^* - \lambda I & & \vdots & K & C \\ & & & -2\lambda a_{2g+n} & & \\ \hline & & & 0 & & \\ & 0 & & \vdots & \bar{\phi}^* - I & D \\ & & & 0 & & \\ \hline & & & 0 & & \\ & 0 & & \vdots & 0 & \bar{\phi}^* - \lambda^{-1} I \\ & & & 0 & & \end{array}\right].$$

Here, $\bar{\phi}^* : H^1(S \setminus \sigma) \to H^1(S \setminus \sigma)$ is the $(2g+n) \times (2g+n)$ matrix describing the

cohomology action induced by ϕ, and can be written as a block matrix

$$\begin{bmatrix} [\phi^*] & 0 \\ 0 & [P] \end{bmatrix}$$

where $P = (p_{ij})$ is a permutation matrix denoting the permutation of the singularities in σ. In particular, if $\tau\delta_j\tau^{-1} = w_j\delta_{k_j}w_j^{-1}$, then $p_{jk_j} = 1$. By the previous lemmas, $\phi^* - \lambda I$ and $\phi^* - \lambda^{-1}I$ have 1 dimensional kernel. Furthermore, since 1 is not an eigenvalue of ϕ^*, $\bar{\phi}^* - I$ has kernel whose dimension is equal to the number of disjoint cycles of the permutation of the punctures. But a cycle in the permutation corresponds to a single boundary component of N. Hence, the kernel of R has dimension at most $2 + m + 1$, where the additional 1 comes from the $(2g + n) + 1$–th column of R and

$$m = \#\text{ of components of } \Sigma = \#\text{ of components of } \partial N.$$

Now consider the upper left portion of the matrix

$$U = \begin{pmatrix} \begin{bmatrix} \\ \bar{\phi}^* - \lambda I \\ \\ \hline \\ 0 \\ \\ \end{bmatrix} & \begin{matrix} -2\lambda a_1 \\ \vdots \\ -2\lambda a_{2g+n} \\ \hline 0 \\ \vdots \\ 0 \end{matrix} & \begin{bmatrix} \\ K \\ \\ \hline \\ \bar{\phi}^* - I \\ \\ \end{bmatrix} \end{pmatrix}.$$

Since the α_i and β_i for $1 \leq i \leq g$ do not intersect $\Pi_{j=1}^{n}\delta_j = \partial D$, we have that $K_{ij} = 0$ for $2g < j \leq 2g + n$. Because any vector $\vec{y}$ in the kernel of $\bar{\phi}^* - I$ comes from the permutation block P (in other words, the ith coordinates y_i zero for $1 \leq i \leq 2g$),

then we have that $K\vec{y} = 0$. Hence, if $\text{null}(U) > 2 + m$, then we must be able to solve

$$(\bar{\phi}^* - \lambda I) \begin{pmatrix} x_1 \\ x_2 \\ \vdots \\ x_{2g+n} \end{pmatrix} = \begin{pmatrix} 2\lambda a_1 \\ \vdots \\ 2\lambda a_{2g+n} \end{pmatrix}.$$

Since λ is a simple eigenvalue of ϕ^* and $(a_1, \ldots, a_{2g})$ is a corresponding eigenvector for λ, the equation has no solutions.

Hence $\text{null}(R) = 2 + m$. However, the solution arising from the kernel of $\bar{\phi}^* - \lambda I$ is the eigenvector

$$\vec{v} = \begin{pmatrix} a_1 \\ \vdots \\ a_{2g+n} \\ 0 \\ \vdots \\ 0 \\ 0 \\ \vdots \\ 0 \end{pmatrix}$$

which is a coboundary, as it is just a multiple of the representation ρ_0. So we have that $\dim H^1(\Gamma, \mathfrak{sl}(2, \mathbb{R})_{\text{Ad}_{\rho_0}}) \leq m + 1$. Finally, there is one further redundancy since

$$\Pi_{i=1}^{g}[\alpha_i, \beta_i] = \Pi_{j=1}^{n}\delta_j.$$

From the $\bar{\phi}^* - I$ block, we can see that $y_{2g+1}, \ldots, y_{2g+n}$ can be freely chosen as long as $y_{2g+j} = y_{2g+k_j}$ whenever $\tau\delta_j\tau^{-1} = w_j\delta_{k_j}w_j^{-1}$. Hence, the upper-left (and lower-right)

entry of $c(\Pi_{j=1}^{n}\delta_j)$ can be freely chosen to be any quantity

$$y_{2g+1} + y_{2g+2} + \dots y_{2g+n}. \tag{4.1}$$

The relation $\Pi_{i=1}^{g}[\alpha_i, \beta_i] = \Pi_{j=1}^{n}\delta_j$ forces the sum in Equation 4.1 to be a fixed quantity coming from the upper-left entry of $\Pi_{i=1}^{g}[\alpha_i, \beta_i]$, which has no dependence on y_{2g+j}, for $1 \leq j \leq n$.

Therefore $\dim H^1(\Gamma, \mathfrak{sl}(2,\mathbb{R})_{\mathrm{Ad}_{\rho_0}}) \leq m$. □

Since $\dim H^1(\Gamma, \mathfrak{sl}(2,\mathbb{R})_{\mathrm{Ad}_{\rho_0}}) = m$, the representation variety is smooth at the representation ρ_0.

4.3 Singular hyperbolic structures

From the proof of Theorem 4.3, we also can find a tangent vector at ρ_0 (i.e. cocycle) corresponding to $\mathcal{F}^s$. λ^{-1} is a simple eigenvalue of $\bar{\phi}^*$ with its eigenvector coming from $\mu_s(\gamma_1), \dots, \mu_s(\gamma_{2g+n})$, which we will denote $b_1, \dots, b_{2g+n}$. By assumption, ϕ^* does not have 1 as an eigenvalue, so we can solve

$$(\phi^* - I)\begin{pmatrix} y_1 \\ \vdots \\ y_{2g} \end{pmatrix} = -D_{2g\times 2g}\begin{pmatrix} b_1 \\ \vdots \\ b_{2g} \end{pmatrix}, \tag{4.2}$$

where $D_{2g\times 2g}$ is the restriction of D to the upper left $2g \times 2g$ entries.

Finally, since λ is a simple eigenvalue of $\bar{\phi}^*$, we can also solve

$$(\bar{\phi}^* - \lambda I)\begin{pmatrix} x_1 \\ \vdots \\ x_{2g+n} \end{pmatrix} - 2\lambda\begin{pmatrix} a_1 \\ \vdots \\ a_{2g+n} \end{pmatrix} y_0 = -K\begin{pmatrix} y_1 \\ \vdots \\ y_{2g+n} \end{pmatrix} - C\begin{pmatrix} b_1 \\ \vdots \\ b_{2g+n} \end{pmatrix}. \tag{4.3}$$

Now we will use the above cocycle, which we will call c_0.

$$c_0(\gamma_i) = \begin{bmatrix} y_i & x_i \\ b_i & -y_i \end{bmatrix}$$
$$c_0(\tau) = \begin{bmatrix} y_0 & 0 \\ 0 & -y_0 \end{bmatrix}$$

We conjugate the representation ρ_0 and its tangent vector $c_0 \cdot \rho_0$ by

$$\mathfrak{r}_1(s) = \begin{bmatrix} s & 0 \\ 0 & \frac{1}{s} \end{bmatrix}.$$

Converting this information into an HP representation gives the representation ρ_{HP}

$$\rho_{HP}(\gamma_i) = \begin{bmatrix} 1 & 0 & 0 & 0 \\ 0 & 1 & 0 & 0 \\ 0 & 0 & 1 & 0 \\ -\frac{b_i}{s^2} + s^2 x_i & -\frac{b_i}{s^2} - s^2 x_i & 2y_i & 1 \end{bmatrix} \begin{bmatrix} 1 + \frac{a_i^2 s^4}{2} & -\frac{a_i^2 s^4}{2} & a_i s^2 & 0 \\ \frac{a_i^2 s^4}{2} & 1 - \frac{a_i^2 s^4}{2} & a_i s^2 & 0 \\ a_i s^2 & -a_i s^2 & 1 & 0 \\ 0 & 0 & 0 & 1 \end{bmatrix}$$
$$= \begin{bmatrix} 1 + \frac{a_i^2 s^4}{2} & -\frac{1}{2} a_i^2 s^4 & a_i s^2 & 0 \\ \frac{a_i^2 s^4}{2} & 1 - \frac{a_i^2 s^4}{2} & a_i s^2 & 0 \\ a_i s^2 & -a_i s^2 & 1 & 0 \\ -\frac{b_i}{s^2} + s^2(x_i + 2a_i y - a_i^2 b_i) & -\frac{b_i}{s^2} - s^2(x_i + 2a_i y - a_i^2 b_i) & -2a_i b_i + 2y_i & 1 \end{bmatrix}$$
$$\rho_{HP}(\tau) = \begin{bmatrix} \frac{1}{2}(\lambda + \lambda^{-1}) & \frac{1}{2}(\lambda - \lambda^{-1}) & 0 & 0 \\ \frac{1}{2}(\lambda - \lambda^{-1}) & \frac{1}{2}(\lambda + \lambda^{-1}) & 0 & 0 \\ 0 & 0 & 1 & 0 \\ 0 & 0 & y_0 & 1 \end{bmatrix}.$$

Conjugating by

$$\mathfrak{r}_2(s) = \begin{bmatrix} 1 & 0 & 0 & 0 \\ 0 & 1 & 0 & 0 \\ 0 & 0 & 0 & -s^2 \\ 0 & 0 & s^{-2} & 0 \end{bmatrix}$$

and taking $s \to 0$ gives the Sol representation

$$\rho_{\mathrm{Sol}}(\gamma_i) = \begin{bmatrix} 1 & 0 & 0 & 0 \\ 0 & 1 & 0 & 0 \\ b & b & 1 & 0 \\ a & -a & 0 & 1 \end{bmatrix}$$

$$\rho_{\mathrm{Sol}}(\tau) = \begin{bmatrix} \frac{1}{2}(\lambda+\lambda^{-1}) & \frac{1}{2}(\lambda-\lambda^{-1}) & 0 & 0 \\ \frac{1}{2}(\lambda-\lambda^{-1}) & \frac{1}{2}(\lambda+\lambda^{-1}) & 0 & 0 \\ 0 & 0 & 1 & 0 \\ 0 & 0 & 0 & 1 \end{bmatrix}.$$

Thus, there is a family of HP representations that limit to the Sol representation in $\mathrm{PGL}(4,\mathbb{R})$, up to rescaling the path of HP structures by $\mathfrak{r}_2(s)$. In order to realize the representation as geometric structures, we will need the Ehresmann-Thurston principle [27].

Theorem 4.4 (Ehresmann-Thurston Principle)**.** *Let X be a manifold upon which a Lie group G acts transitively. Let M have a (X,G)-structure with holonomy representation $\rho : \pi_1(M) \to G$. For ρ' sufficiently near ρ in the space of representations $Hom(\pi_1(M), G)$, there exists a nearby (X,G)- structure on M with holonomy representation ρ'.*

Theorem 4.5. *Let $\phi : S \to S$ be a pseudo-Anosov homeomorphism whose stable and*

unstable foliations, $\mathcal{F}^s$ and $\mathcal{F}^u$, are orientable and ϕ^* does not have 1 as an eigenvalue. Then, there exists a family of singular hyperbolic structures on M_ϕ, smooth on the complement of Σ, that degenerate to a transversely hyperbolic foliation. The degeneration can be rescaled so that the path of rescaled structures limit to the singular Sol structure on M_ϕ, as projective structures.

Proof. Notice that all of the structure groups for HP, $\mathbb{H}^3$, and Sol can be written as subgroups of $\mathrm{PGL}(4,\mathbb{R})$, giving them $(\mathbb{R}P^3, \mathrm{PGL}(4,\mathbb{R}))$-structures. Since the Sol representation, as a representation into $\mathrm{PGL}(4,\mathbb{R})$ comes from an actual Sol structure on N, then by Theorem 4.4, the HP representations correspond to robust HP structures in a neighborhood of the Sol representation.

Work of Danciger [6] then says that in a neighborhood of each HP structure, we have a family of $\mathbb{H}^3$ (and AdS) structures $\rho_{t,s}$ that degenerate to a transversely hyperbolic foliation, with the transversely hyperbolic foliation obtained by conjugating ρ_0 by $\mathfrak{r}_1(s)$. Rescaling the degeneration by some $\mathfrak{r}_{t,s}$ yields the HP structure. Fix an $s = s_0$, and a family of hyperbolic structures given by their holonomy representations ρ_{t,s_0}. Conjugating ρ_{t,s_0} by $\mathfrak{r}_1(ss_0^{-1})$ yields a family $\rho_{t,s}$ whose rescaled limit is ρ_{HP}, with the rescaling maps $\mathfrak{r}_{t,s}$ also obtained by conjugating $\mathfrak{r}_{t,s_0}$ by $\mathfrak{r}_1(ss_0^{-1})$. Since $\mathfrak{r}_1(s) \in \mathrm{PSL}(2,\mathbb{R})$, conjugation does not change the underlying geometric structure on M_ϕ, and each of the $\rho_{t,s}$ limit to equivalent transversely hyperbolic foliations. Composing the rescalings $\mathfrak{r}_{t,s}$, $\mathfrak{r}_1(s)$, and $\mathfrak{r}_2(s)$, we can find a path of singular hyperbolic structures that collapse to the structure given by ρ_0 so that a rescaling of the degeneration by the composition gives the Sol structure. □

Note that the cocycle c_0 has the property that

$$c_0(\gamma_i) = \begin{bmatrix} y_i & x_i \\ b_i & -y_i \end{bmatrix},$$

where $b_i = \mu_s(\gamma_i)$. In particular, the deformation of ρ_0 contains the information of $\mathcal{F}^s$. More specifically, if c_0 were of the form

$$c_0(\gamma_i) = \begin{bmatrix} 0 & 0 \\ b_i & 0 \end{bmatrix},$$

then c_0 would deform the trivial representation to the lower triangular representation

$$\rho' = \begin{bmatrix} 1 & 0 \\ b_i & 1 \end{bmatrix}.$$

While c_0 does not quite have this form, we can see that in some sense, the deformation from the upper triangular representation ρ_0, which is a projection onto $\mathcal{F}^u$, is in the direction of $\mathcal{F}^s$.

4.4 The behavior of the singularities

We can see from the method of regenerating hyperbolic structures that the singular hyperbolic structure is related to the natural singular Sol geometry on M_ϕ. In particular, the HP representations that limit to the Sol representation come from the $\mathbb{H}^2$ representation of projecting onto $\mathcal{F}^s$ along with a tangent vector c_0 containing the information of transverse direction. In order to further understand the singular hyperbolic structures, it will be helpful to understand the behavior of the singularities Σ.

We can think of $N = M_\phi \setminus \Sigma$ as a manifold with torus boundary components. Let m be a meridian curve encircling one of the boundary components, and l an longitudinal curve. In Danciger [6], it is shown that if the HP representation can be

conjugated so that

$$\rho_{HP}(m) = \begin{bmatrix} 1 & 0 & 0 & 0 \\ 0 & 1 & 0 & 0 \\ 0 & 0 & 1 & 0 \\ 0 & 0 & \omega & 1 \end{bmatrix},$$

$$\rho_{HP}(l) = \begin{bmatrix} \cosh d & \sinh d & 0 & 0 \\ \sinh d & \cosh d & 0 & 0 \\ 0 & 0 & \pm 1 & 0 \\ 0 & 0 & \mu & \pm 1 \end{bmatrix},$$

then the nearby hyperbolic structures that degenerate to the HP structure (after rescaling) have a cone singularity about that particular component of Σ. In particular, take the family of representations into SO(3,1) such that

$$\rho_t(m) = \begin{bmatrix} 1 & 0 & 0 & 0 \\ 0 & 1 & 0 & 0 \\ 0 & 0 & \cos \omega t & -\sin \omega t \\ 0 & 0 & \sin \omega t & \cos \omega t \end{bmatrix},$$

$$\rho_t(l) = \begin{bmatrix} \cosh d & \sinh d & 0 & 0 \\ \sinh d & \cosh d & 0 & 0 \\ 0 & 0 & \pm \cos \mu t & -\sin \mu t \\ 0 & 0 & \sin \mu t & \pm \cos \mu t \end{bmatrix}.$$

Then, conjugating by

$$\begin{bmatrix} 1 & 0 & 0 & 0 \\ 0 & 1 & 0 & 0 \\ 0 & 0 & 1 & 0 \\ 0 & 0 & 0 & t^{-1} \end{bmatrix}$$

and taking the limit as $t \to 0$ yields $\rho_{HP}(m)$ and $\rho_{HP}(l)$. Thus, ω, which Danciger calls the *infinitesimal cone angle*, describes the infinitesimal change in the cone angle about that component of the singularity.

In the case that Σ has multiple components, as in our case, we can modify the computation. We begin by finding the HP matrix for the same situation except conjugated by some isometry in $\mathrm{Isom}(\mathbb{H}^3)$. Conjugate $\rho_t(m)$ and $\rho_t(l)$ by

$$\begin{bmatrix} 1+\frac{a^2}{2} & -\frac{a^2}{2} & a & 0 \\ \frac{a^2}{2} & 1-\frac{a^2}{2} & a & 0 \\ a & -a & 1 & 0 \\ 0 & 0 & 0 & 1 \end{bmatrix},$$

which is the matrix in $\mathrm{SO}(3,1)$ corresponding to the parabolic isometry

$$\begin{bmatrix} 1 & a \\ 0 & 1 \end{bmatrix} \in \mathrm{PSL}(2,\mathbb{C}).$$

If we then conjugate by

$$\begin{bmatrix} 1 & 0 & 0 & 0 \\ 0 & 1 & 0 & 0 \\ 0 & 0 & 1 & 0 \\ 0 & 0 & 0 & t^{-1} \end{bmatrix}$$

and take the limit as $t \to 0$, we get the HP matrix

$$\rho_{HP}(m) = \begin{bmatrix} 1 & 0 & 0 & 0 \\ 0 & 1 & 0 & 0 \\ 0 & 0 & 1 & 0 \\ -\omega \operatorname{Re} a & \omega \operatorname{Re} a & \omega & 1 \end{bmatrix}, \tag{4.4}$$

$$\rho_{HP}(l) = \begin{bmatrix} \mp a^2 + (1+a^2)\cosh d & \pm a^2 - a^2 \cosh d + \sinh d & a(\pm 1 - \cosh d - \sinh d) & 0 \\ \mp a^2 + a^2 \cosh d + \sinh d & \pm a^2 + (1-a^2)\cosh d & a(\pm 1 - \cosh d - \sinh d) & 0 \\ a(\cosh d - \sinh d \mp 1) & a(\sinh d \pm 1 - \cosh d) & \pm 1 & 0 \\ -a\mu & a\mu & \mu & \pm 1 \end{bmatrix}. \tag{4.5}$$

Hence, the ω entry still gives the infinitesimal cone angle, and the left two entries in the bottom row of $\rho_{HP}(m)$ describe the amount that the axis of the cone singularity has been translated (parabolically). We can see that $\rho_{HP}(\delta_j)$ has the form of $\rho_{HP}(m)$, and $\rho_{HP}(\tau)$ has the form of $\rho_{HP}(l)$, so we have cone-type singularities along Σ.

A computation of the commutator $\rho_{HP}([\alpha_i, \beta_i])$ yields a matrix of the form in Equation 4.4:

$$\begin{bmatrix} 1 & 0 & 0 & 0 \\ 0 & 1 & 0 & 0 \\ 0 & 0 & 1 & 0 \\ -s^2 f & s^2 f & g & 1 \end{bmatrix},$$

where f and g are in terms of $a_i, a_{g+i}, b_i, b_{g+i}$.

Therefore, the product of the commutators $\rho_{HP}(\Pi_{i=1}^{g}[\alpha_i, \beta_i])$ also has this form.

In the case where $\gamma_{2g+j} = \delta_j$, we also have that

$$\rho_{HP}(\delta_j) = \rho_{HP}(\gamma_{2g+j}) = \begin{bmatrix} 1 & 0 & 0 & 0 \\ 0 & 1 & 0 & 0 \\ 0 & 0 & 1 & 0 \\ s^2 x_{2g+j} & -s^2 x_{2g+j} & 2y_{2g+j} & 1 \end{bmatrix}.$$

Note that $y_{2g+j} = y_{2g+j'}$ if δ_j and $\delta_{j'}$ belong in the same cycle of the permutation (i.e. they are meridians for the same component of Σ). In other words, we have cone-type singularities that develop in the singular hyperbolic structure, and for each component of Σ, there is freedom in choosing the infinitesimal cone angle about that component. Moreover, the commutator/puncture relation

$$\Pi_{i=1}^{g}[\alpha_i, \beta_i] = \Pi_{j=1}^{n}\delta_j$$

says that the sum of the infinitesimal cone angles about each component, weighted by the number of punctures in the permutation for that component, must equal the total infinitesimal cone angle for the loop $\Pi_{i=1}^{g}[\alpha_i, \beta_i]$ that encircles all of the punctures.

Outside of the disk D containing the punctures, the deformation, up to first order, appears like a deformation of a single cone singularity. In other words, instead of considering each puncture separately, the first order behavior is as if we remove the fibers over the disk D to obtain a 3-manifold N' with only one boundary component, with a cone singularity about $\partial N'$. The location of the axis for this singularity is determined by some function of the infinitesimal cone angles about each component of Σ along with the relative locations of the axes for those components.

Proposition 4.6. *The infinitesimal cone angle ω_{tot} of N' is non-zero.*

Proof. A straight-forward computation shows that the $4, 3$ entry in the commutator

$\rho_{HP}([\alpha_i, \beta_i])$ is given by $2(a_i b_{g+i} - a_{g+i} b_i)$. Hence, the $4,3$ entry in the product

$$\rho_{HP}(\Pi_{i=1}^{g}[\alpha_i, \beta_i])$$

is the algebraic intersection pairing $\hat{i}(\vec{e}_\lambda, \vec{e}_{\lambda^{-1}})$.

Suppose e_μ is an eigenvector of ϕ^* with eigenvalue $\mu \neq \lambda$. Then

$$\hat{i}(\vec{e}_\mu, \vec{e}_{\lambda^{-1}}) = \hat{i}(\phi^* \vec{e}_\mu, \phi^* \vec{e}_{\lambda^{-1}}) = \mu\lambda^{-1}\hat{i}(\vec{e}_\mu, \vec{e}_{\lambda^{-1}}).$$

Since $\mu \neq \lambda$, this means that $\hat{i}(\vec{e}_\mu, \vec{e}_{\lambda^{-1}}) = 0$.

If $\vec{e}_{\mu,p}$ is a generalized eigenvector such that $(\phi^* - \mu I)^p \vec{e}_{\mu,p} = 0$, then we induct on p. Notice that $\phi^* \vec{e}_{\mu,p} = \mu \vec{e}_{\mu,p} + c\vec{e}_{\mu,p-1}$, where $(\phi^* - \mu I)^{p-1} \vec{e}_{\mu,p-1} = 0$. Hence, if $\hat{i}(\vec{e}_{\mu,p-1}, \vec{e}_{\lambda^{-1}}) = 0$, then it must be that $\hat{i}(\vec{e}_{\mu,p}, \vec{e}_{\lambda^{-1}}) = 0$ as well since

$$\hat{i}(\vec{e}_{\mu,p}, \vec{e}_{\lambda^{-1}}) = \hat{i}(\phi^* \vec{e}_{\mu,p}, \phi^* \vec{e}_{\lambda^{-1}}) = \mu\lambda^{-1}\hat{i}(\vec{e}_{\mu,p}, \vec{e}_{\lambda^{-1}}).$$

The generalized eigenvectors of ϕ^* span $\mathbb{R}^{2g}$ and λ is a simple eigenvalue, so that means that if $\hat{i}(\vec{e}_\lambda, \vec{e}_{\lambda^{-1}}) = 0$, then $\hat{i}(\vec{u}, \vec{e}_{\lambda^{-1}}) = 0$ for all $\vec{u} \in \mathbb{R}^{2g}$, contradicting the non-degenerate condition for symplectic forms. □

4.5 Genus 2 example

We will compute the representations and parameters to find the deformation in a genus two example. Begin with the curves $\alpha_1, \alpha_2, \beta_1, \beta_2$, which form the symplectic basis for $H_1(S)$. We begin with left Dehn twists $T_{\beta_1}, T_{\beta_2}, T_\gamma$ along β_1, β_2, and γ, followed by right Dehn twists $T_{\alpha_1}^{-1}, T_{\alpha_2}^{-1}$ along α_1 and α_2. Since the disjoint sets of curves $\{\alpha_1, \alpha_2\}$ and $\{\beta_1, \beta_2, \gamma\}$ fill, the resulting homeomorphism $\phi : S \to S$ is pseudo-Anosov.

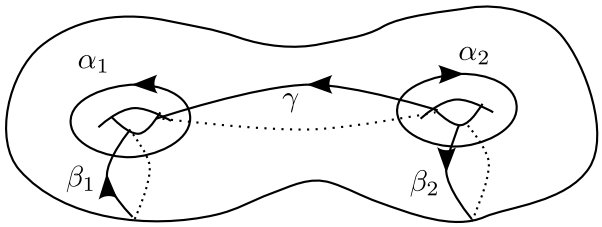

Figure 4.1: The curves $\alpha_1, \alpha_2, \beta_1, \beta_2$ which form the symplectic basis for $H_1(S)$, and γ.

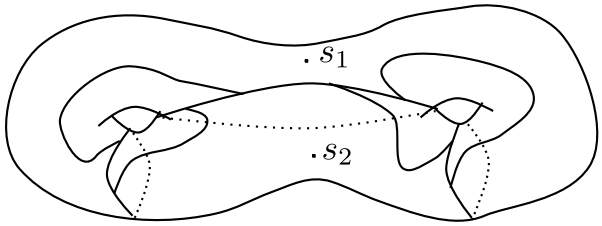

Figure 4.2: A train track for $\mathcal{F}^u$.

The stable and unstable foliations are orientable with two singular points of cone angle 4π, one in each of the two components of $S \setminus \{\alpha_1, \alpha_2, \beta_1, \beta_2, \gamma\}$. A train track for the $\mathcal{F}^u$ is shown in Figure 4.2, and we can verify that the foliations are orientable with two singularities s_1 and s_2.

The induced action on cohomology, with the generators $\alpha_1, \alpha_2, \beta_1, \beta_2$, is

$$\phi^* = \begin{bmatrix} 3 & 1 & 2 & 1 \\ 1 & 3 & 1 & 2 \\ 1 & 0 & 1 & 0 \\ 0 & 1 & 0 & 1 \end{bmatrix}.$$

The matrix is Perron-Frobenius, with largest eigenvalue $\lambda_1 = \frac{5+\sqrt{21}}{2}$. The other

eigenvalue $\lambda_2 > 1$ is given by $\lambda_2 = \frac{3+\sqrt{5}}{2}$. The eigenvectors of ϕ^* for λ_1 and λ_1^{-1} are

$$\vec{e}_{\lambda_1} = \begin{pmatrix} \frac{3+\sqrt{21}}{2} \\ \frac{3+\sqrt{21}}{2} \\ 1 \\ 1 \end{pmatrix}$$
$$\vec{e}_{\lambda_1^{-1}} = \begin{pmatrix} \frac{\sqrt{21}-3}{2} \\ \frac{\sqrt{21}-3}{2} \\ -1 \\ -1 \end{pmatrix}.$$

We have a choice for $\vec{e}_{\lambda_1^{-1}}$ as it is only unique up to scale. We make the choice that is consistent with the orientation of the embedding of Sol into $\mathbb{R}^4$. In particular, in the standard embedding, the x-coordinate is contracted and the y-coordinate is expanded. Our choice for $\vec{e}_{\lambda_1}$ and $\vec{e}_{\lambda_1^{-1}}$ has the same orientation in the singular flat metric on S.

Thus, we obtain the parameters

$$a_1 = a_2 = \frac{3+\sqrt{21}}{2}$$
$$a_3 = a_4 = 1$$
$$b_1 = b_2 = \frac{\sqrt{21}-3}{2}$$
$$b_3 = b_4 = -1.$$

Fix a basepoint and choose representatives for $\alpha_1, \alpha_2, \beta_1, \beta_2$ in $\pi_1(S)$, which we will also call $\alpha_1, \alpha_2, \beta_1, \beta_2$ (see Figure 4.3). We can then compute the action of ϕ on $\pi_1(S)$:

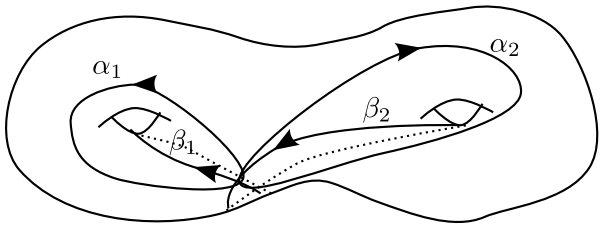

Figure 4.3: Generators for $\pi_1(S)$.

$$\phi(\alpha_1) = \alpha_1\beta_1\beta_2\alpha_2\alpha_1^2\beta_1$$
$$\phi(\alpha_2) = \alpha_1\beta_1\beta_2\alpha_2^2\beta_2\alpha_2$$
$$\phi(\beta_1) = \alpha_1\beta_1$$
$$\phi(\beta_2) = \beta_2\alpha_2.$$

In addition, taking generators δ_1 and δ_2 for loops around the singularities s_1 and s_2, we have the following action of ϕ on $\pi_1(S \setminus \sigma)$:

$$\phi(\delta_1) = \beta_1\beta_2\delta_1\beta_2^{-1}\beta_1^{-1}$$
$$\phi(\delta_2) = \delta_2,$$

with $a_5 = a_6 = b_5 = b_6 = 0$.

Thus, we have that

$$D = \begin{bmatrix} \frac{23+5\sqrt{21}}{2} & \frac{7+\sqrt{21}}{2} & \frac{19+5\sqrt{21}}{2} & \frac{5+\sqrt{21}}{2} & 0 & 0 \\ 0 & 16+3\sqrt{21} & \frac{3+\sqrt{21}}{2} & 9+2\sqrt{21} & 0 & 0 \\ 0 & 0 & \frac{3+\sqrt{21}}{2} & 0 & 0 & 0 \\ 0 & 1 & 0 & 0 & 0 & 0 \\ 0 & 0 & 0 & 0 & 2 & 0 \\ 0 & 0 & 0 & 0 & 0 & 0 \end{bmatrix}$$

$$C = -\begin{bmatrix} \frac{271+59\sqrt{21}}{2} & \frac{35+7\sqrt{21}}{2} & \frac{311+67\sqrt{21}}{2} & \frac{23+5\sqrt{21}}{2} & 0 & 0 \\ 0 & 167+36\sqrt{21} & \frac{15+3\sqrt{21}}{2} & 101+22\sqrt{21} & 0 & 0 \\ 0 & 0 & \frac{15+3\sqrt{21}}{2} & 0 & 0 & 0 \\ 0 & 1 & 0 & 0 & 0 & 0 \\ 0 & 0 & 0 & 0 & 4 & 0 \\ 0 & 0 & 0 & 0 & 0 & 0 \end{bmatrix},$$

and $K = -2D$.

From this, we calculate from Equation 4.2 that

$$\begin{pmatrix} y_1 \\ y_2 \\ y_3 \\ y_4 \end{pmatrix} = -(\phi^* - I)^{-1} D_{4\times 4} \begin{pmatrix} b_1 \\ b_2 \\ b_3 \\ b_4 \end{pmatrix} = \begin{pmatrix} \frac{3+\sqrt{21}}{2} \\ \frac{3-\sqrt{21}}{2} \\ -\frac{3+\sqrt{21}}{6} \\ -\frac{3+\sqrt{21}}{6} \end{pmatrix},$$

and y_5 and y_6 are free. The span of $\phi^* - \lambda_1 I$ is generated by the first three columns, so we can take $x_4 = 0$ (taking $x_4 \neq 0$ would change the solution by a co-boundary).

We then compute the other x_i and y_0 from Equation 4.3, yielding

$$\begin{aligned} x_1 &= -\frac{27+5\sqrt{21}}{3} \\ x_2 &= \frac{15+\sqrt{21}}{3} \\ x_3 &= 0 \\ x_4 &= 0 \\ x_5 &= \frac{2-2\sqrt{21}}{3} y_5 \\ x_6 &= 0 \\ y_0 &= \frac{\sqrt{21}}{6}. \end{aligned}$$

The 4,3 entry in the commutator $\rho_{HP}([\alpha_i, \beta_i])$ is computed to be $2(a_i b_{2+i} - a_{2+i} b_i)$. Hence, the total infintesimal cone angle ω_{tot} is equal to $-4\sqrt{21}$. (Because of the choice for generators of π_1, the curve around the punctures is actually $[\beta_1^{-1}, \alpha_1][\alpha_2, \beta_2]$, but gives the same answer for ω_{tot}.) The infinitesimal cone angles about the two boundary components should add up to $\omega_{tot} = -4\sqrt{21}$. Hence, the infinitesimal cone angles can be chosen so that the cone angles about both singularities are decreasing towards 2π. By scaling the b_i by a positive scalar, it is also possible to change ω_{tot} to any negative number.

Chapter 5

Ideal Triangulations

5.1 Hyperbolic ideal tetrahedra

One way to describe a hyperbolic 3-manifold with cusps is to realize it as a set of ideal hyperbolic tetrahedra glued together along faces. Using the upper half-space model for $\mathbb{H}^3$, we can, up to isometry, place three of the four ideal vertices of a tetrahedron at 0, ∞, and 1. The fourth vertex will then be somewhere on the boundary plane, and its complex coordinate, z, indicates the isometry class of the terahedron. This complex number, z, is the *(complex) shape parameter* of the tetrahedron. The shape parameter also represents the complex dihedral angle along the edge from 0 to ∞.

For an arbitrary ideal tetrahedron with vertices at a, b, c, d in the complex plane, the shape parameter can be calculated as the cross ratio $z = (a, b; c, d) = \frac{(a-c)(b-d)}{(b-c)(a-d)}$, which corresponds to the complex dihedral angle along the edge between a and b [27]. In the case where z is strictly real, the tetrahedron has been flatted onto a hyperbolic plane, and we say that the tetrahedron is *degenerate*.

If we glue tetrahedra together along faces, then we can find an algebraic condition for the triangulation by looking at all of the tetrahedra which share the same edge. Picking an edge e, number tetrahedra as T_1, $T_2, \ldots, T_k$ as we go counter-clockwise

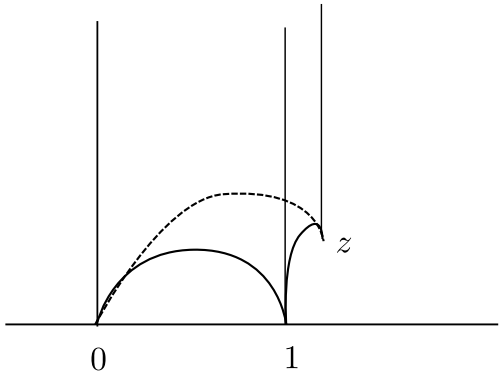

Figure 5.1: Ideal tetrahedron in the upper half-space model with vertices at 0, 1, ∞, and z

around the e, and assign complex shape parameters $z_1, z_2, \ldots, z_k$, respectively. We can realize T_1 as a hyperbolic ideal tetrahedron with vertices at $0, \infty, 1$, and z_1. Then, we take T_2 to be a tetrahedron with complex shape parameter z_2, with vertices at $0, \infty, z_1, z_1 z_2$, so that the $0, \infty, z_1$ faces of T_1 and T_2 are identified. We can continue to develop tetrahedra in this manner, and the condition that the final face of T_k matches the first face of T_1 is that $z_1 z_2 \cdots z_k = 1$. In addition, in order for the total angle around each edge to be equal to 2π, we must have that $\operatorname{Im} z_1 + \operatorname{Im} z_2 + \cdots + \operatorname{Im} z_k = 2\pi$. For each edge in the triangulation, we obtain one of these *edge consistency equations*. The solution space to the set of all edge consistency equations forms the *deformation variety* of hyperbolic structures realized by the triangulation.

Agol [1] describes a way of triangulating the mapping torus M_ϕ using triangulations on the surface S dual to the maximal splitting sequence of an invariant train track. Let τ be a train track for $\mathcal{F}^s$. Any two train tracks for $\mathcal{F}^s$ are equivalent up to a sequence of splitting and folding moves [23], which are shown in Figure 5.2.

A key observation by Agol is that any two train tracks for $\mathcal{F}^s$ have a common *maximal splitting*. A maximal splitting is a splitting along branches with the largest weight. This, unlike the more classical Penner result, gives a canonical sequence of

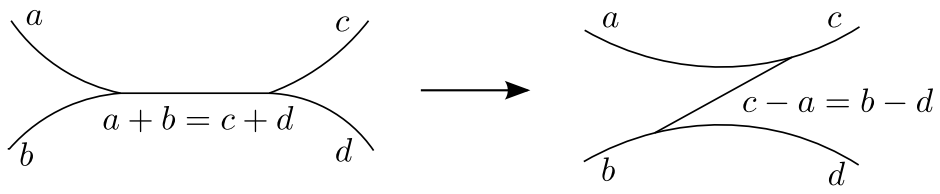

Figure 5.2: A splitting of a branch on a train track. The reverse operation is called a fold.

splittings.

Theorem 5.1 (Agol [1], Corollary 3.4)**.** *Let τ and τ' be two train tracks for $\mathcal{F}^s$. Then τ and τ' have a common maximal splitting. That is, if $\tau = \tau_0, \tau_1, \tau_2, \tau_3, \ldots$ is the sequence of train tracks obtained from maximal splittings on τ, and $\tau' = \tau'_0, \tau'_1, \tau'_3, \ldots$ is the sequence of train tracks obtained from maximal splittings of τ', then there exists m, n so that $\tau_m = \tau_n$, up to isotopy.*

Applying Theorem 5.1 to τ and $\phi(\tau)$ then yields eventual periodicity of a maximal splitting sequence.

Theorem 5.2 (Agol [1], Theorem 3.5)**.** *Let $\tau = \tau_0, \tau_1, \tau_2, \tau_3, \ldots$ be the sequence of maximal splittings for train tracks for $\mathcal{F}^s$. Then, there exists m, n so that $\tau_{m+n} = \lambda^{-1}\phi(\tau_m)$.*

Since the switches of the train track are trivalent, the dual graph to a train track on S is a triangulation of S. Each splitting move on the train track corresponds to a Whitehead move on the triangulation, which can be interpreted as gluing a tetrahedron onto the triangulation (see Figure 5.3). In this way, a triangulation for the manifold is built up in layers, and the periodicity means that eventually, the top layer can be glued onto the bottom layer by the homeomorphism ϕ. Notice that the vertices are in bijective correspondence with the complementary regions of τ. Each complementary region of a train track represents a singularity of the invariant

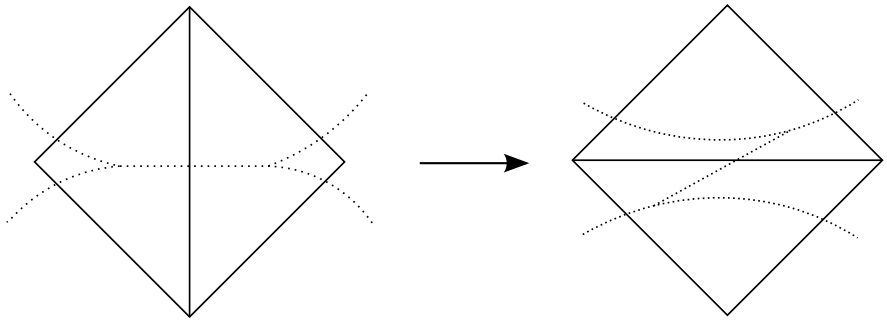

Figure 5.3: A Whitehead move is dual to a splitting of a train track, and a Whitehead move determines a tetrahedron.

foliations. In other words, each vertex of the triangulation is a singularity of the foliation, so the resulting ideal triangulation is a triangulation of $N_\phi = M_\phi \setminus \Sigma$, where Σ is the locus of singular fibers (the fibers over the singularities σ). Additionally, the construction endows a natural taut angle structure on the triangulation where the diagonals in Figure 5.3 have angle π, and the sides of the quadrilateral have angle 0.

An important property of the triangulation of N_ϕ is that it is veering. Given an edge e in a triangulation coming from Agol's construction, we can consider the triangles which have e as an edge.

Definition 5.3. An edge e in a triangulation is *left-veering* if in the layering from the Agol triangulation, the vertices opposite e are moving to the left as we go up from triangle to triangle. An edge is *right-veering* if they move to the right.

Definition 5.4. A triangulation is *veering* if every edge in the triangulation is either left-veering or right-veering.

Theorem 5.5 (Agol [1])**.** *A taut ideal triangulation of a fibered manifold coming from Whitehead moves is associated to a periodic splitting sequence if and only if it is veering.*

This theorem suggests that the combinatorics of a veering triangulation contains

the information about the train tracks in the periodic splitting sequence. From the periodic splitting sequence, it is a simple matter to obtain the foliations $\mathcal{F}^{s/u}$ along with their respective transverse measures $\mu_{s/u}$. Furthermore, since the maximal splitting sequence is canonical, the ideal triangulation for N_ϕ from this construction is also canonical. Even if we start with two unique train tracks for $\mathcal{F}^s$, because they have a common maximal splitting, the maximal splitting sequences for each train track will eventually stabilize to the same periodic sequence of train tracks.

5.2 Angle structures

Hodgson, Rubinstein, Segerman, and Tillman [18], and Futer and Guéritaud [10] prove the existence of angle structures on these veering triangulations where all of the angles are strictly between 0 and π. We prove some additional results on angle structures and the existence of corresponding geometric solutions to Thurston's gluing equations.

As in Futer and Guéritaud [10], we will assign the shape parameters z_i to the diagonals of the taut ideal tetrahedra, where the i indicates the tetrahedron corresponding to the ith splitting in the maximal splitting sequence. The coloring convention of Hodgson, Rubinstein, Segerman, and Tillman [18] and Futer and Guéritaud [10] of right veering edges being red and left veering edges being blue will be used as shown in Figure 5.4.

Every edge e in the Agol taut ideal triangulation has two tetrahedra with shape parameters which are of the z_i type along e. If e is a right veering edge, then all shape parameters along the edge e for all other tetrahedra are of the x_j type, so the Thurston edge consistency equations have the form

$$z_{i_0} x_{j_0} x_{j_2} \cdots x_{j_m} z_{i_1} x_{k_n} x_{k_{n-1}} \cdots x_{k_0} = 1.$$

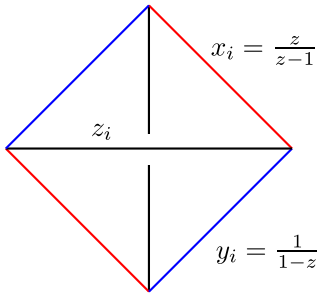

Figure 5.4: Flattened tetrahedron with diagonals having shape parameter z_i, the red edges being right veering with shape parameter x_i, and the blue edges being left veering with shape parameter y_i.

In terms of the layering coming from the maximal splitting sequence, here, z_{i_0} corresponds to the shape parameter of the bottom-most tetrahedron T_0 touching e, i.e. the tetrahedron in which e is the top diagonal created after splitting along a maximal branch. Then, using the terminology of Futer and Guéritaud, there are two fans on each side of e. Hodgson, Rubinstein, Segerman, and Tillman show that each fan is non-empty [18, Lemma 2.3]. On one side, we have a sequence of tetrahedron contributing shape parameters of x_{j_0}, x_{j_1}, ..., x_{j_m} from the bottom to the top, and on the other side x_{k_0}, x_{k_1}, ..., x_{k_n}, starting from the tetrahedron directly above T_0. Eventually, e will be split, leaving another tetrahedron who bottom diagonal is e and contributing a shape parameter of z_{i_1}. A similar thing holds for left veering edges, with x's replaced by y's.

Proposition 5.6. *There exists no (real) solution to the Thurston edge consistency equations for veering triangulations with $z_i < 0$ for all i.*

Proof. Notice that if $z_i < 0$, then

$$|y_i| = \left|\frac{1}{1 - z_i}\right| < 1$$

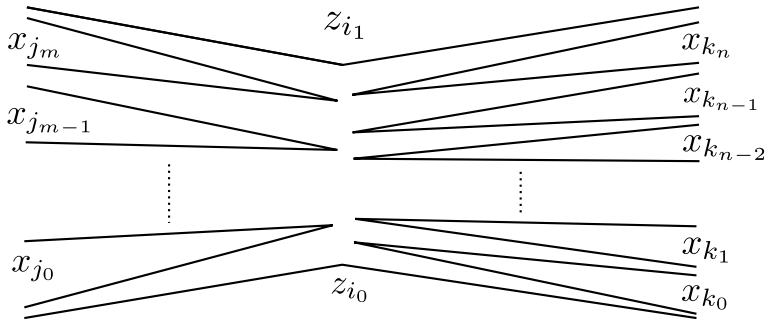

Figure 5.5: Edge consistency equation around a right veering edge has two fans of x's sandwiched between two z's.

and also

$$|z_i y_i| = \left| \frac{z_i}{1 - z_i} \right| < 1.$$

By the previous observation, if we multiply together the gluing consistency equations for all of the left veering edges, then we will obtain a product consisting of all of the y_i (twice) and some of the z_i, with each z_i having multiplicity at most two. In other words, we must satisfy the equation

$$\prod_{i \in I} y_i^2 \prod_{j \in J \subset I} z_j^{l_j} = 1$$

where $I = 0, \ldots, n$ indexes the tetrahedra in the Agol triangulation and $l_j \in \{1, 2\}$. The left-hand side has absolute value less than 1 when $z_i < 0$ for all $i \in I$, so the edge consistency equations cannot be satisfied. □

A solution with $z_i < 0$ for all i corresponds to a π angle on all of the diagonals of the flattened tetrahedra from Agol's construction – in other words, the natural taut angle structure. Hence, Proposition 5.6 shows that there is no real solution to the edge consistency equations with angles prescribed by the natural taut angle structure coming from the diagonal exchange moves on the surface.

We now demonstrate another canonical taut angle structure. The notions of "above" and "below" the z_i angles are well-defined by the layering induced by the maximal splitting sequence.

Proposition 5.7. *There exist angle structures on veering triangulations such that the π angles are precisely the top angles in each fan (in other words, the two angles directly "above" the angles which are π in the angle structure induced from the taut ideal triangulation; e.g. in Figure 5.5, the angles x_{j_m} and x_{k_n}) or precisely the two bottom angles in each fan (e.g. x_{j_0} and x_{k_0} in Figure 5.5), with all other angles equal to 0.*

Proof. Around each edge e of the triangulation, picking the two angles which are at the top of each of the two fans to have angle π gives a total angle of 2π around the edge. So it remains to check that such a choice is well-defined and each ideal tetrahedron has exactly one of its shape angles equal to π, with the others 0.

First we check that if a tetrahedron T is the topmost in a fan along an edge e, then T is also the topmost in the fan along the edge f opposite e in T. We label the other edges of the quadrilateral determining the tetrahedron T by a and b, with the top diagonal labeled as c. Without loss of generality, assume e and f are right veering (red), and a and b are left veering (blue). Then, c is a right veering edge as in Figure 5.6. Since T is the topmost tetrahedron in the fan at edge e, then in the next tetrahedron up, e is involved in a diagonal exchange for some quadrilateral containing edges a and c. We label the other edges of this quadrilateral d and g as in Figure 5.6.

Now consider the edge c. On the right-hand side of c is a fan containing the tetrahedron determined by the quadrilateral $acgd$. Since both fans must be non-empty, then before c is replaced by a diagonal exchange, there must be a tetrahedron T' layered on top of the left-hand side of c. Furthermore, the tetrahedron will have triangle bcf as a face. Hence, it must be that either b or f is the diagonal of T'. But

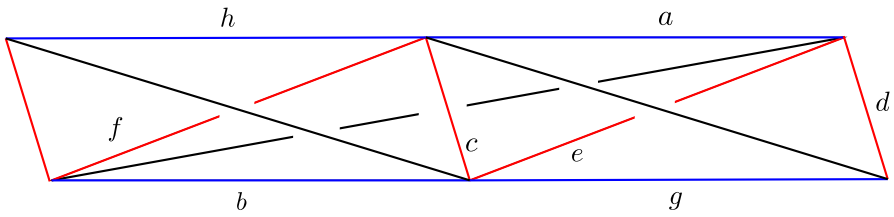

Figure 5.6: The tetrahedron T given by $afbe$ with T' layered above bcf and $\bar{T}$ above ace. Veering forces specific diagonal exchanges.

c and f are right veering (red) and b is left veering (blue), so it must be that f is the lower diagonal of T'. In other words, T is the topmost tetrahedron is the fan about f.

From the argument above, it also follows that T' is above T in the fan about the edge b, so the dihedral angle for T about b is 0. Similarly, the tetrahedron determined by $acgd$ lies above T in the fan about a, so the only dihedral angle for T that is π is x_i.

Conversely, if the tetrahedron T determined by the quadrilateral $afbe$ is not the topmost tetrahedron in the fan about a, there exists another tetrahedron $\bar{T}$ above T in the fan about the edge a. Without loss of generality, assume a is left veering (blue). Then in $\bar{T}$, the diagonal that is exchanged is e, so that c is right veering (red). We can then repeat the previous argument to see that there is a tetrahedron T' above T in the fan about b, and we also see that T is the topmost tetrahedron in the fans about e and f, forcing the x_i dihedral angle to be π.

Hence, the choice of the topmost angles in the fan to be π gives a well-defined taut angle structure on the veering triangulation. The argument that choosing the bottommost angles in each fan to be π gives a taut angle structure follows similarly.

□

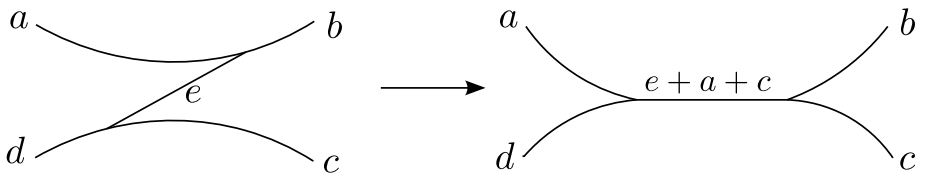

Figure 5.7: Measured train track and corresponding transverse measure after a fold.

5.3 Real solutions to edge consistency equations

We now demonstrate a method for finding real solutions to the edge consistency equations whose dihedral angles correspond to one of the two canonical angle structure solutions given in the previous section. The real solution described in the current section has dihedral angles equal to π for the topmost angles in a fan.

Suppose we are given a veering layered taut ideal triangulation. By Agol [1, Proposition 4.2], by choosing an immersed triangulated surface, we can recover the maximal splitting sequence of train tracks. From the splitting sequence, it is a fairly simple procedure to determine the invariant projective measure μ on the track τ for the pseudo-Anosov element ϕ. For simplicity, we work with the folding sequence instead of the splitting sequence. Given a measured train track and a fold, the measure on the folded edge can be written as a sum of the measures of the branches involved in the fold as in Figure 5.7. Given a periodic folding sequence, we can find the measures of each branch after one period as a linear combination of the measures of the branches in the original track.

By Agol [1, Theorem 3.5], the measure μ' on τ after one period in the folding sequence is $\lambda(\phi)\phi(\tau)$ where $\lambda(\phi) > 1$ is the pseudo-Anosov dilatation factor of ϕ. Hence, the transition matrix of the folding sequence is Perron-Frobenius, and the largest eigenvalue is $\lambda(\phi)$ with the corresponding eigenvector giving the invariant projective measure μ.

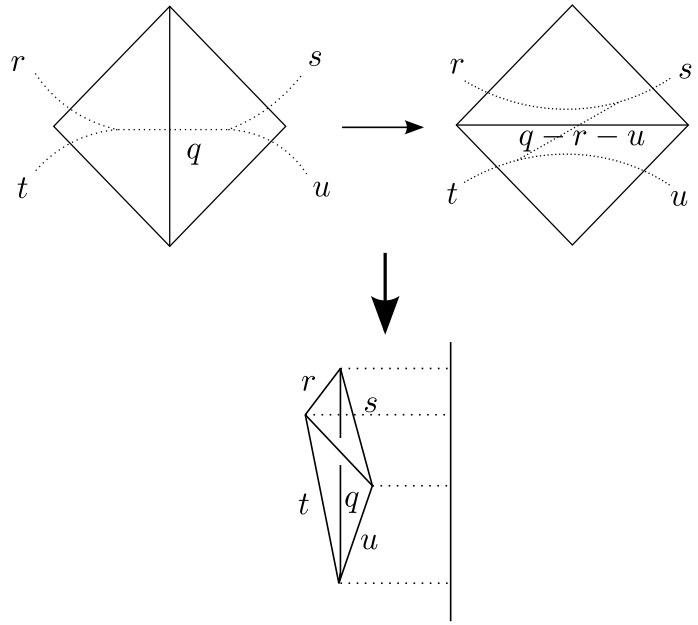

Figure 5.8: Obtaining a flattened tetrahedron using the measure from the dual train track.

Consequently, given the Agol triangulation for the mapping torus M_ϕ of a pseudo-Anosov mapping class ϕ, we can assume that we have the dual maximal splitting sequence along with the measures on the train tracks at each stage. With this information, we demonstrate how to determine real solutions to the edge consistency equations. To obtain a solution to the edge consistency equations, we will use the measured train track.

Consider a maximal large branch q as in Figure 5.8. When the branch q is split, a tetrahedron is formed via diagonal exchange. Each edge in the tetrahedron is dual to a weighted branch of the measured train track, and we can assign lengths to each of the edges by taking the length to equal the measure of dual branch. The switch conditions $q = r + t = s + u$, $r + (q - r - u) = s$), and $t = (q - r - u) + u$ determine a projection of the tetrahedron onto $\mathbb{R}$, up to translation. Hence, this determines an ideal hyperbolic tetrahedron collapsed onto $\mathbb{H}^2$. We can find the corresponding (real)

shape parameter z_i of the tetrahedron by sending the bottom vertex to 0, the top vertex to q, and the left vertex to 1 on $\partial\mathbb{H}^2$ and taking the cross ratio

$$z_i = (q, 0; t, u) = \frac{(q-t)(0-u)}{(0-t)(q-u)} = \frac{u(q-t)}{t(q-u)} = \frac{ur}{ts}.$$

Notice that if $t > u$ – i.e. we have a left split – then $0 < z_i < 1$ so that $x_i < 0$. In other words, x_i has an angle of π. On the other hand, if $t < u$, i.e. we have a right split, then $z_i > 1$ so that $y_i < 0$ and y_i has an angle of π. Also, the bottom diagonal is always the longest edge, as it is dual to a maximally weighted branch.

The above procedure determines real-valued shape parameters for all tetrahedra in the Agol triangulation of M_ϕ. We show that the prescribed shape parameters satisfy the edge consistency equations.

Theorem 5.8. *The assignment of shape parameters to tetrahedra using the projection to $\mathbb{R} \subset \partial\mathbb{H}^2$ using the weights of the dual branch as the $\mathbb{R}$-lengths of the edges gives a solution to the edge consistency equations where the π angles are at the topmost tetrahedra in each fan.*

Proof. Consider a fan of an edge e. Without loss of generality, we assume e is right veering. A triangle in the veering triangulation corresponds to a switch, and looking at the $\mathbb{R}$ projection of the triangle, the longest edge in the projection is the half-branch that is large (see Figure 5.9). Thus, if we look at the sequence of triangles (which are veering to the right) incident to e, as long as the longest edge of the projected triangle is not e, then the edge incident to the right endpoint of e is the longest edge, so will be part of a diagonal exchange, and the triangles will continue to be layered on tp of it, veering to the right as in Figure 5.10. When the largest edge in the triangle is e, then branch dual to e will split, and e will be replaced by another edge in a diagonal exchange.

If we label the projection of one endpoint of e as 0 with the other endpoint being

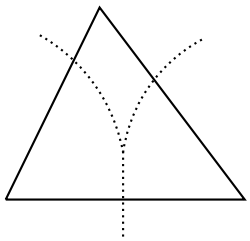

Figure 5.9: The $\mathbb{R}$ projection can be seen as the projection onto a horizontal line. The bottom edge has the largest length and corresponds to the large half-branch.

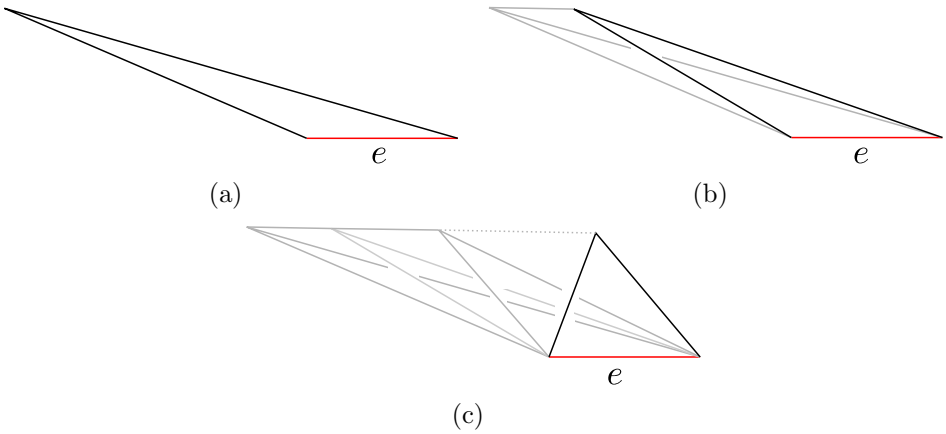

Figure 5.10: Triangles are layered along e, veering to the right as long as the vertex opposite e lies to the left of the left endpoint of e.

q, where q is the weight of the branch dual to e, then the projections of the vertices opposite e in one fan of e satisfy

$$a_0 < a_1 < a_2 < \cdots < a_{m-1} < 0 < a_m < q$$

where the ordering of the indices respects the ordering of the layering of the triangles. Likewise, the vertices opposite e in the other fan satisfy

$$0 < b_n < q < b_{n-1} < b_{n-2} < \cdots < b_2 < b_1 < b_0.$$

From this projection, we can see that the holonomy around the edge is 1 so that the gluing consistency equation at e is satisfied. The shape parameter associated to the dihedral angle at e for the flattened tetrahedron determined by $0, q, a_0$ and a_1 takes the segment between 0 and a_0 to the segment between 0 and a_1. Then the shape parameter for the tetrahedron determined by $0, q, a_1, a_2$ takes the segment from 0 to a_1 to the segment from 0 to a_2, and so on, until the shape parameter for the tetrahedron determined by the vertices $0, q, a_{m-1}, a_m$ takes a_{m-1} to a_m. Then the shape parameter for the top tetrahedron determined by $0, q, a_m, b_n$ takes a_m to b_n. The sequence of shape parameters in the lower fan in Figure 5.11 then takes b_n to b_{n-1}, b_{n-1} to b_{n-2}, and on to b_0. Then the shape parameter for the tetrahedron determined by $0, q, a_0, b_0$ then takes b_0 back to a_0.

Algebraically, this can be verified by computing the shape parameters from the cross ratios. The shape parameter about the edge e for the bottom tetrahedron is

$$(q, 0; b_0, a_0) = \frac{a_0(q - b_0)}{b_0(q - a_0)}.$$

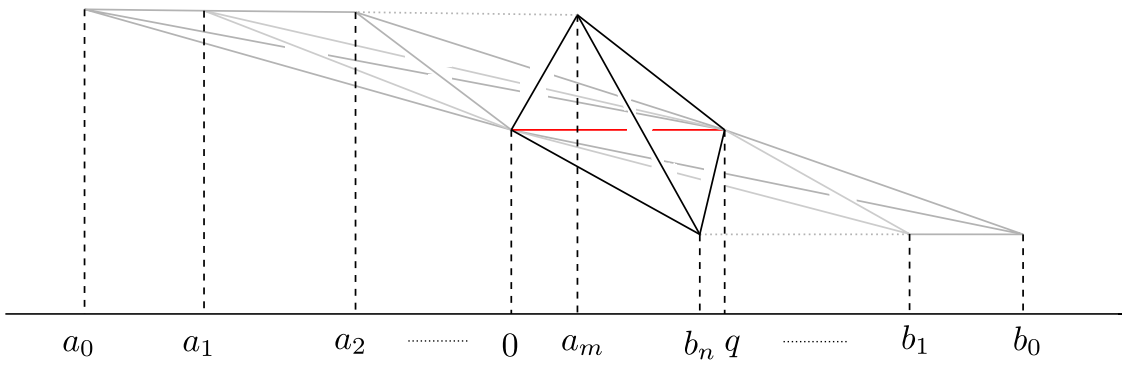

Figure 5.11: The projection onto $\mathbb{R}$ at e, with the projections of the vertices opposite e denoted by a_i and b_j.

Along the fan above e in Figure 5.11, the respective shape parameters about e are

$$(q, 0; a_i, a_{i+1}) = \frac{a_{i+1}(q - a_i)}{a_i(q - a_{i+1})}.$$

For the top tetrahedron, the shape parameter, when given a consistent orientation with the above, is given by

$$(q, 0; a_m, b_n) = \frac{b_n(q - a_m)}{a_m(q - b_n)}$$

while the shape parameters along the fan below e in Figure 5.11 are

$$(q, 0; b_i, b_{i-1}) = \frac{b_{i-1}(q - b_i)}{b_i(q - b_{i-1})}.$$

Then, the product of all of the shape parameters is

$$\frac{a_0(q - b_0)}{b_0(q - a_0)} \frac{a_1(q - a_0)}{a_0(q - a_1)} \frac{a_2(q - a_1)}{a_1(q - a_2)} \cdots \frac{a_m(q - a_{m-1})}{a_{m-1}(q - a_m)} \frac{b_n(q - a_m)}{a_m(q - b_n)}$$
$$\frac{b_{n-1}(q - b_n)}{b_n(q - b_{n-1})} \frac{b_{n-2}(q - b_{n-1})}{b_{n-1}(q - b_{n-2})} \cdots \frac{b_0(q - b_1)}{b_1(q - b_0)} = 1.$$

The above computations of the shape parameters also shows that the only two angles which are π (i.e. the shape parameters are strictly negative) are from the topmost tetrahedron in each fan, since the given cross ratios are negative only when $a_i < 0$ and $a_{i+1} > 0$ or when $b_i < q$ and $b_{i+1} > q$. □

5.4 Deformation of tetrahedra

We would like to deform the real solution for the edge consistency equations to obtain a solution where the tetrahedra have positive volume (i.e. the imaginary parts of the shape parameters are strictly positive). In other words, given shape parameters

$$x_1, y_1, z_1, x_2, y_2, z_2, \ldots, x_n, y_n, z_n$$

and edge consistency equations

$$\begin{aligned} g_1(z_1, z_2, \ldots, z_n) &= 1 \\ g_2(z_1, z_2, \ldots, z_n) &= 1 \\ &\vdots \\ g_n(z_1, z_2, \ldots, z_n) &= 1, \end{aligned}$$

we want a path of parameters $\{z_i(t)\}$ such that

$$\begin{aligned} g_1(z_1(t), z_2(t), \ldots, z_n(t)) &= 1 \\ g_2(z_1(t), z_2(t), \ldots, z_n(t)) &= 1 \\ &\vdots \\ g_n(z_1(t), z_2(t), \ldots, z_n(t)) &= 1, \end{aligned}$$

such that for $t > 0$, $\mathrm{Im}(z_i(t)) > 0$.

To simplify the analysis, we will consider $d \log g_i$ as in Choi [4] and Danciger [6]. For indices i such that $x_i < 0$ in the real solution, define $\xi_i = d \log x_i$ and $c_i = z_i$ so that

$$\begin{aligned} d \log x_i &= \xi_i \\ d \log y_i &= -c_i \xi_i \\ d \log z_i &= -(1 - c_i)\xi_i. \end{aligned}$$

For indices i such that $y_i < 0$, define $\xi_i = d \log y_i$ and $c_i = \frac{1}{z_i}$ so that

$$\begin{aligned} d \log x_i &= -c_i \xi_i \\ d \log y_i &= \xi_i \\ d \log z_i &= -(1 - c_i)\xi_i. \end{aligned}$$

Notice that by our choice of c_i, $0 < c_i < 1$. We can now write our system of edge consistency equations as

$$A\xi = 0 \tag{5.1}$$

where $\xi = (\xi_1, \xi_2, \ldots, \xi_n)^T$ and A is a $n \times n$ matrix. The kernel of A, then, is the Zariski tangent space to the variety defined by the gluing equations g_i. To compute the dimension of this kernel, we will consider A^T.

Because the i-th tetrahedron contributes two x_i's, two y_i's, and two z_i's to the edge consistency equations, the i-th column of A contains two 1 entries, two $-c_i$ entires, and two $-(1 - c_i)$ entries, or sums of the 1, $-c_i$ and $-(1 - c_i)$ where each type of coefficient appears in exactly twice as summands (possibly in different sums).

Hence, if we let $r = (r_1, r_2, \ldots, r_n)^T$ be a vector, then the jth coordinate of $A^T r$ is

$$r_a + r_b - c_j(r_d + r_e) - (1 - c_j)(r_k + r_l)$$

where a, b, d, e, k, l are not necessarily distinct. The kernel of A^T can then be re-written as the solution to $n + 1$ equations of the form

$$(r_a + r_b) - (r_k + r_l) = c_j[(r_d + r_e) - (r_k + r_l)].$$

By definition of ξ_i, r_a and r_b correspond to the edges of the j-th tetrahedron that have angle π (i.e. negative shape parameter). Hence, if we have that $(r_a+r_b)-(r_k+r_l) \neq 0$, and hence, $(r_d + r_e) - (r_k + r_l) \neq 0$, then we must have either

$$r_d + r_e > r_a + r_b > r_k + r_l$$

or

$$r_k + r_l > r_a + r_b > r_d + r_e \tag{5.2}$$

since $0 < c_j < 1$. Otherwise, $r_a + r_b = r_d + r_e = r_k + r_l$.

Applying a result of Choi [4, Theorem 3.7(ii)], for each cusp in the veering triangulation, there is a non-trivial vector in the kernel of A^T. We reproduce a version of the argument applicable to our situation here.

Proposition 5.9. *Let c be a cusp of the veering triangulation and $e_{i_1}, \ldots, e_{i_k}$ ideal edges of the triangulation with c as an endpoint (with multiplicity). Then the vector*

$$v = \boldsymbol{e}_{i_1} + \cdots + \boldsymbol{e}_{i_k}$$

is in the kernel of A^T, where $\boldsymbol{e}_i$ is the standard unit basis vector $(0, \ldots, 0, 1, 0, \ldots, 0)$ that is 1 in the ith coordinate and 0 in all other coordinates.

Proof. We have a triangulation of the cusp c induced from the tetrahedralization of the mapping torus by cutting off a neighborhood of the ideal vertex to obtain triangles "at infinity". The ith coordinate $v_{(i)}$ of the vector v is $d\log$ of the product of all of the x_i, y_i, and z_i that appear in the cusp c. But the x_i, y_i, and z_i appear together as a triple for each vertex of the tetrahedron T_i that lies on the cusp c. Since $x_i y_i z_i \equiv -1$, then $d\log(x_i y_i z_i) = 0$. $v_{(i)}$ is a sum of some number of $d\log(x_i y_i z_i)$, so $v_{(i)} = 0$. □

Assuming we can show that $r_a + r_b = r_d + r_e = r_k + r_l$, from the argument in Choi [4, Theorem 3.7(iii)], then the kernel of A^T consists of only those relations coming from the cusps. The argument is reproduced below.

Proposition 5.10. *Suppose that $A^T r = 0$ and for each tetrahedron in the ideal triangulation*

$$r_a + r_b = r_d + r_e = r_k + r_l,$$

where $\{r_a, r_b\}$, $\{r_d, r_e\}$, $\{r_k, r_l\}$ are weights assigned to pairs of opposite edges of the tetrahedron. Then r is a linear combination of the vectors in the kernel of A^T from Proposition 5.9.

Proof. For a cusp c_j, let v_j be the vector from Proposition 5.9. We wish to find a

$$q = \sum_{c_j \text{ a cusp}} q_j v_j$$

such that $q = r$. We write q as

$$q = \sum_i (q_{a_i} + q_{b_i})\mathbf{e}_i,$$

where q_{a_i} and q_{b_i} are the two ends of the edge e_i. Then, the equations that the q_j and r_i must satisfy are

$$q_{a_i} + q_{b_i} = r_i.$$

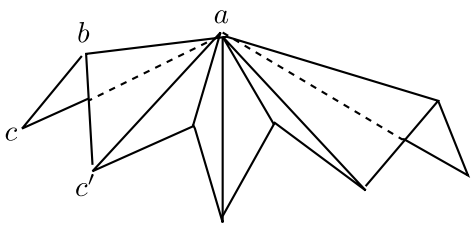

Figure 5.12: Traversing along adjacent faces of tetrahedra to go between two triangles sharing a common vertex a.

If we consider three vertices a, b, c of a face on a tetrahedron with edges e_{ab}, e_{ac}, e_{bc}, then we have the three equations

$$q_a + q_b = r_{i_{ab}}$$
$$q_a + q_c = r_{i_{ac}}$$
$$q_b + q_c = r_{i_{bc}}.$$

This has solutions

$$q_a = \frac{r_{i_{ab}} - r_{i_{bc}} + r_{i_{ac}}}{2}$$
$$q_b = \frac{r_{i_{ab}} - r_{i_{ac}} + r_{i_{bc}}}{2}$$
$$q_c = \frac{r_{i_{ac}} - r_{i_{ab}} + r_{i_{bc}}}{2}.$$

It remains to show that the q_j are well-defined. Suppose two faces of two tetrahedra share a vertex a. Then we can go from one to another through a sequence of faces so that two consecutive faces are faces of the same tetrahedron, as in Figure 5.12. So it suffices to show that the definition of q_a along two triangular faces of a single tetrahedron agree.

Let (a, b, c) be the vertices of one and (a, b, c') be the vertices of the other. Then,

we must show that

$$\frac{r_{i_{ab}} - r_{i_{bc}} + r_{i_{ac}}}{2} = \frac{r_{i_{ab}} - r_{i_{bc'}} + r_{i_{ac'}}}{2}.$$

By assumption, we have that

$$r_{i_{ac}} + r_{i_{bc'}} = r_{i_{ac'}} + r_{i_{bc}},$$

so q_a is well-defined. □

Thus, in order to show that the variety of solutions to the edge consistency equations is smooth, we must show that the relation $r_a + r_b = r_d + r_e = r_k + r_l$ holds. Then, given a vector v in the kernel of A, we can find a family of shape parameters $z_i(t)$ that satisfy the edge consistency equations where the infitesimal change in the $z_i(t)$ at $t = 0$ is given by v.

5.5 The punctured torus case

We consider the special case when $S = S_{1,1}$ is the punctured torus. The hyperbolic structures for the mapping tori coming from pseudo-Anosov elements on $S_{1,1}$ are understood by the work of Guéritaud [12]. As an example of the method outlined above, we will deform the real solution to the gluing equations given by Theorem 5.8 to find positively oriented ideal tetrahedra triangulating the mapping torus M_ϕ.

First, observe that up to the action of the mapping group, there is a unique train track on the flat torus (in the square picture of the torus, let the puncture be located in the corners – which are identified). Since the train track contains two switches and one large branch, the corresponding veering triangulation of $S_{1,1}$ has two triangles. Splitting the large branch corresponds to a Dehn twist, and the veering triangulation from Agol's construction yields the monodromy triangulation studied by Guéritaud [12]. Note that opposite edges of the quadrilateral are identified, so the inequalities

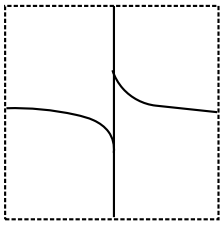

Figure 5.13: Train track on the square punctured torus.

in Equation 5.2 are replaced with

$$2r_d > 2r_a > r_k + r_l$$

or

$$r_k + r_l > 2r_a > 2r_d. \tag{5.3}$$

Here, r_a corresponds to the two opposite edges (which are identified) that are assigned dihedral angle π by Theorem 5.8, r_d is the other pair of opposite edges, and r_k and r_l are the diagonals of the tetrahedron whose edges are assigned shape parameters z_i.

If $2r_a > r_k + r_l$, without loss of generality (by re-labeling r_k and r_l, if necessary), we have that $r_a > r_k$. Similarly, $r_k + r_l > 2r_a$ implies $r_k > r_a$.

In order to prove the smoothness of the deformation variety, we first discuss the structure of the cusp, as described in Gueritaud [12]. The relevant parts are noted below.

By looking at the link of a vertex, we obtain a triangulation of the cusp – each ideal vertex of an ideal tetrahedron contributes a Euclidean triangle to the link of the vertex. These triangles glue together to give a triangualtion of the torus at the cusp. In particular, each tetrahedron contributes four triangles to the cusp, and (in an abuse of notation) the vertices of the triangles can be labeled x_j, y_j, z_j in accordance to the labels given to the edges of the tetrahedron. The labels x_j, y_j, z_j of the vertices

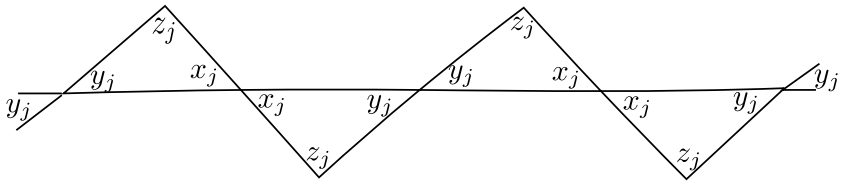

Figure 5.14: Four triangles from the same tetrahedron in the link of cusp.

of the triangles are angles, whereas they are $\mathbb{C}$-valued for edges of the tetrahedron.

As the pair of edges labeled x_j and the pair of edges labeled y_j in the tetrahedron are glued together, the four triangles from each tetrahedron are glued together along their vertices as in Figure 5.14.

Sets of four triangles strung together as in Figure 5.14 are stacked on top of each other to form the triangulation of the torus at the cusp. Note that the x_j labeled vertices come from right veering edges, and the y_j labeled vertices come from the left veering edges.

Proposition 5.11. *The vector on the cusp from Proposition 5.9 is a basis for the kernel of A^T.*

Proof. The idea of the proof is to draw arrows on the edges of the triangulation of the torus at the cusp. For example, if $r_d \geq r_a$, then we draw an arrow on the edge from the vertex x_j (or y_j) to the vertex y_j (or x_j) where x_j (or y_j) corresponds to the edge of r_d and y_j (or x_j) corresponds to the edge of r_l. We make an initial choice of the inequalities on one of the tetrahedra, and show that this forces an orientation of the edges of all other tetrahedra, and the arrows form a cycle so that all coefficients must be equal (this corresponds to the vector v_c from Proposition 5.9).

We first consider a hinge tetrahedron T_{i_1} where the x_{i_1} are at the bottom of the fans of a right veering edge and the y_{i_1} are at the top of the fans of a left veering edge, as in Figure 5.15. In other words, the angle that is π in T_{i_1} from Theorem 5.8 is y_{i_1}. In Equations 5.3, r_a corresponds to the edges with shape parameter y_{i_1}, r_d

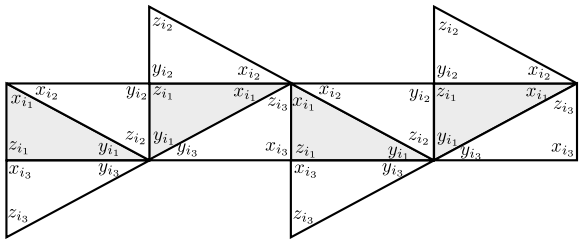

Figure 5.15: A hinge tetrahedron (in gray) where the x_{i_1} are at the bottom of their respective fans and the y_{i_1} are at the top of their fans.

corresponds to the edges with shape parameter x_{i_1}, and r_k and r_l correspond to the two opposite edges of T_{i_1} with shape parameter z_{i_1}. We will refer to the coefficients by the corresponding shape parameters of the vertices in the monodromy triangulation (i.e. the edges in the tetrahedron), so that $r_a = r_{y_{i_1}}$, $r_d = r_{x_{i_1}}$, $r_k = r_{z_{i_1,1}}$, $r_l = r_{z_{i_1,2}}$, etc.

Case HN1: $2r_{x_{i_1}} \leq 2r_{y_{i_1}} \leq r_{z_{i_1,1}} + r_{z_{i_1,2}}$ In this case, we have that $r_{x_{i_1}} \leq r_{y_{i_1}}$, so that we can draw an arrow from y_{i_1} to x_{i_1} along all edges connecting vertices with those labels. Moreover, since

$$2r_{y_{i_1}} \leq r_{z_{i_1,1}} + r_{z_{i_1,2}},$$

we must have either $r_{y_{i_1}} \leq r_{z_{i_1,1}}$ or $r_{y_{i_1}} \leq r_{z_{i_1,2}}$, which takes us to Case HN1a (Figure 5.16) or Case HN1b (Figure 5.17).

In Case HN1a, we see that the choice of arrows on the hinge tetrahedron also places arrows on some of the edges in the adjacent tetrahedron T_{i_2}. In particular, we have that $r_{y_{i_2}} \geq r_{x_{i_2}}$, as in Figure 5.16(b). Also, the angle that is π in T_{i_2} is y_{i_2}. Hence, we must have either $r_{y_{i_2}} \leq r_{z_{i_2,1}}$ or $r_{y_{i_2}} \leq r_{z_{i_2,2}}$. But from the arrows in Figure 5.16(b), we see that $r_{y_{i_2}} \geq r_{z_{i_2,\alpha}}$ for $\alpha = 1$ or $\alpha = 2$, so we must have $r_{y_{i_2}} \geq r_{z_{i_2,\beta}}$ where $\beta = 1$ if $\alpha = 2$ and $\beta = 2$ if $\alpha = 1$.

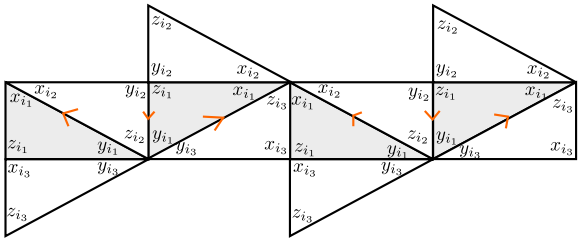

(a)

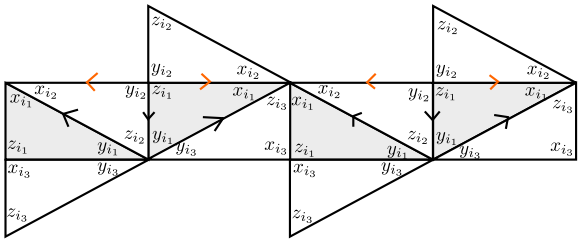

(b)

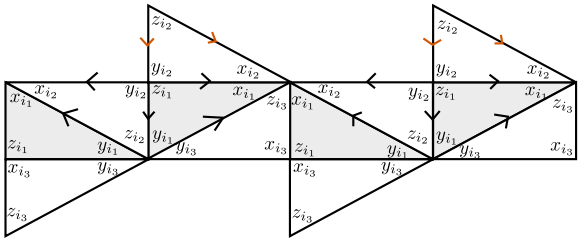

(c)

Figure 5.16: Case HN1a

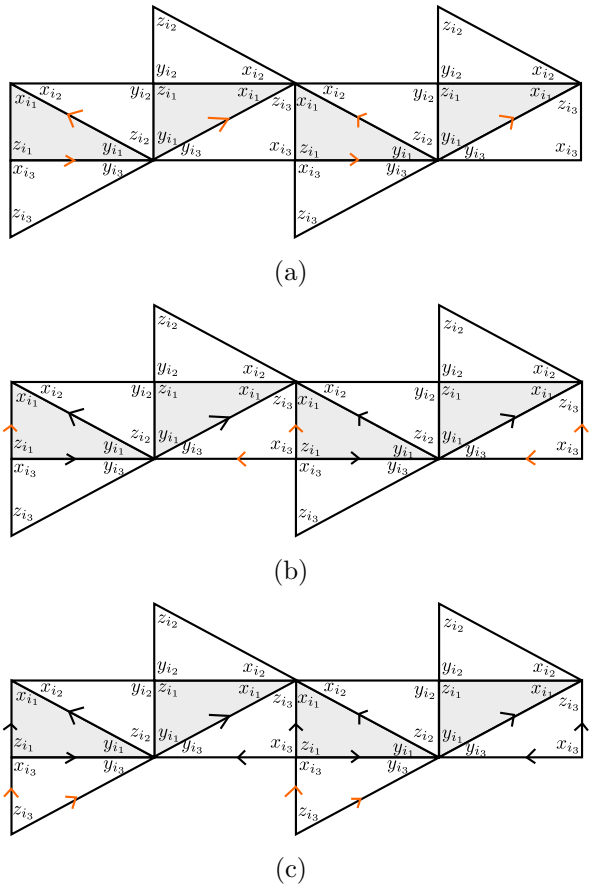

Figure 5.17: Case HN1b

Case HN1b (Figure 5.17) follows similarly, with the choice of arrows on T_{i_1} inducing some of the arrows on T_{i_3}. Here, the angle that is π is x_{i_3}.

Case HN2: $r_{z_{i_1,1}} + r_{z_{i_1,2}} \leq 2r_{y_{i_1}} \leq 2r_{x_{i_1}}$

Case HN2a (Figure 5.18) and Case HN2b (Figure 5.19) follow similar arguments as in Case HN1a and Case HN1b.

We now consider a non-hinge T_{i_2} that occurs in a fan of a right veering edge to another non-hinge T_{i_4}. Notice that the angles that are π in T_{i_2} and T_{i_4} are y_{i_2} and y_{i_4}, respectively.

Case NN1: $2r_{x_{i_2}} \leq 2r_{y_{i_2}} \leq r_{z_{i_2,1}} + r_{z_{i_2,2}}$

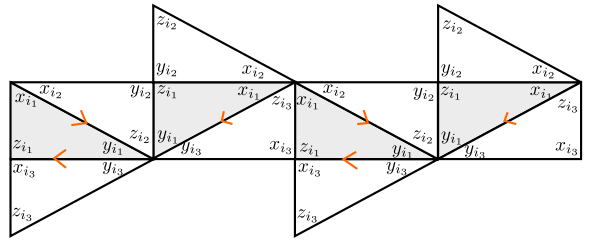

(a)

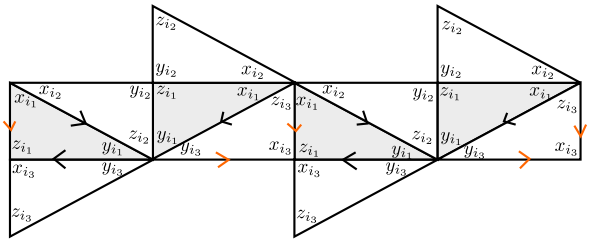

(b)

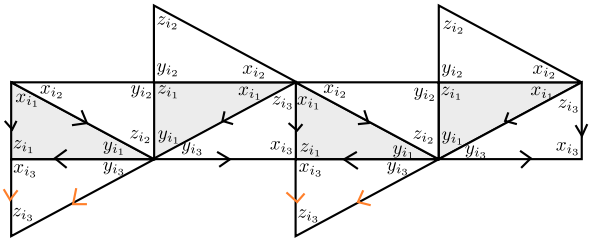

(c)

Figure 5.18: Case HN2a

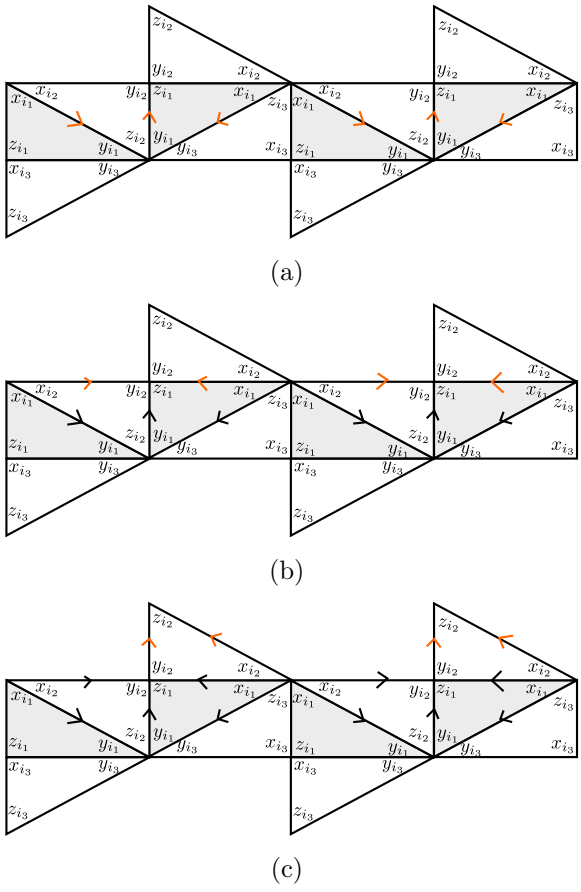

Figure 5.19: Case HN1b

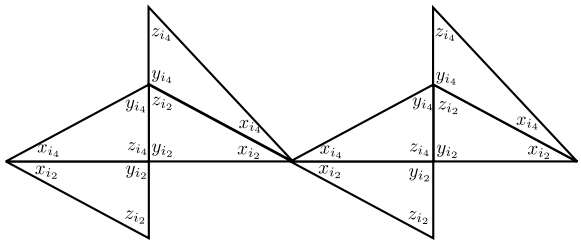

Figure 5.20: A non-hinge tetrahedron in a fan of x_i's neighboring a non-hinge tetrahedron.

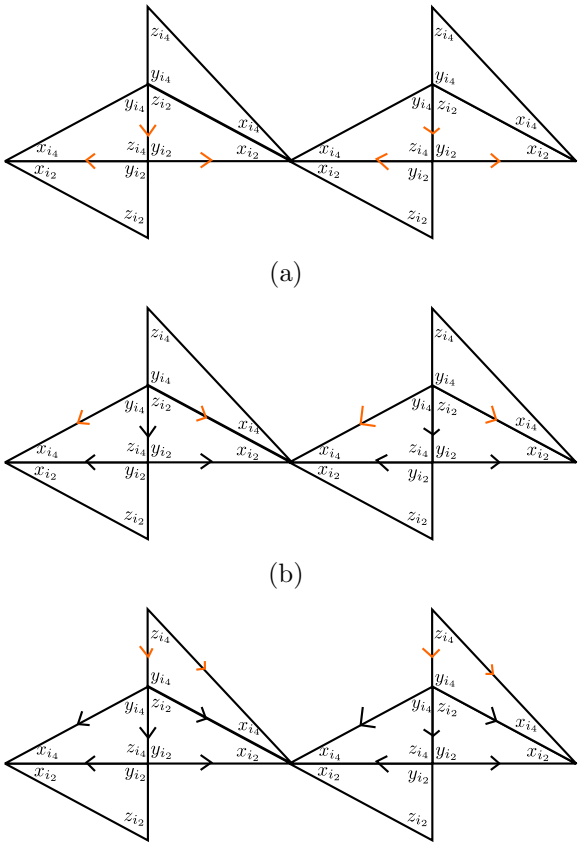

Figure 5.21: Case NN1a

We consider the subcase NN1a when the arrows are as in Figure 5.21.

Case NN2: $r_{z_{i_2,1}} + r_{z_{i_2,2}} \leq 2r_{y_{i_2}} \leq 2r_{x_{i_2}}$

Again, we only consider the subcase NN2a where the arrows are as in Figure 5.22.

Finally, we may have a non-hinge T_{i_2} in a fan of a right veering edge adjacent to a hinge tetrahedron T_{i_4}.

Case NH1: $2r_{x_{i_2}} \leq 2r_{y_{i_2}} \leq r_{z_{i_2,1}} + r_{z_{i_2,2}}$

We consider the subcase NH1a when the arrows are as in Figure 5.24.

Case NH2: $r_{z_{i_2,1}} + r_{z_{i_2,2}} \leq 2r_{y_{i_2}} \leq 2r_{x_{i_2}}$

Again, we only consider the subcase NH2a where the arrows are as in Figure 5.25.

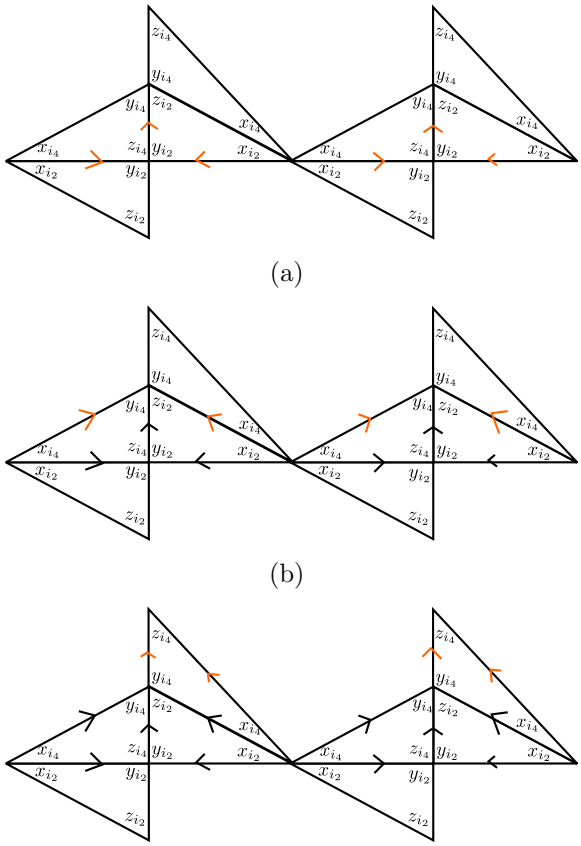

Figure 5.22: Case NN2a

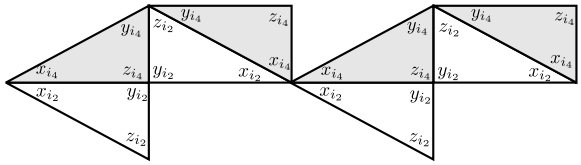

Figure 5.23: A non-hinge tetrahedron in a fan of x_i's neighboring a hinge tetrahedron.

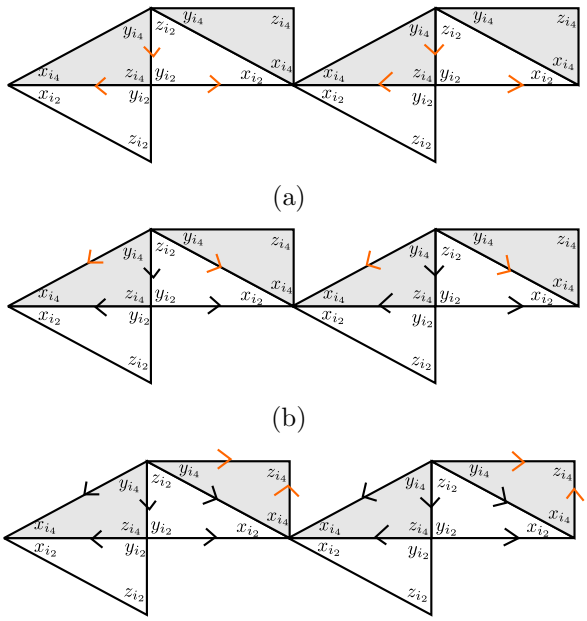

(a)

(b)

(c)

Figure 5.24: Case NH1a

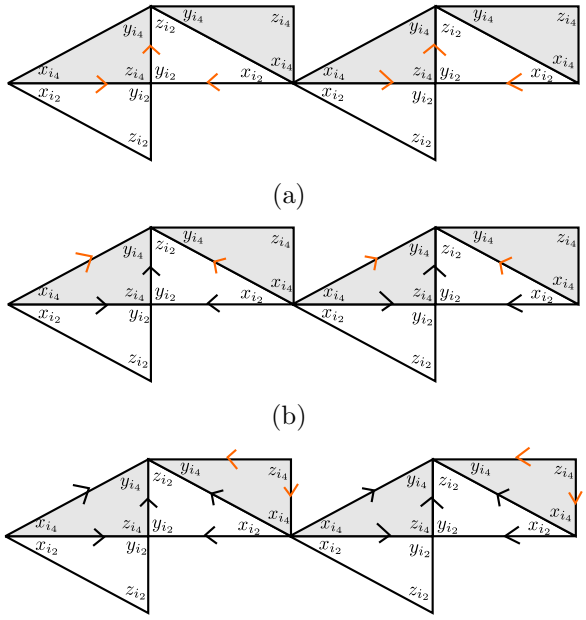

(a)

(b)

(c)

Figure 5.25: Case NH2a

We now proceed to show that the only element in the kernel of A^T is the vector with all entries equal. First, start at any hinge where the x angles are at the bottom of x fans and the y angles are at the top of y fans, as in Figure 5.15. Suppose that we have the situation in Case HN1a. Then, in T_{i_2}, we have edges oriented as in Case NN1a. We can then propogate the arrows upwards along tetrahedra until we reach another hinge tetrahedron as in Case NH1a. Now, we have an orientation on a non-hinge that is in a fan with y_i's. Notice that this picture is a horizontal reflection of the orientation of the hinge tetrahedron in Case HN2a.

Case HN2a proceeds similarly, with the orientation on the non-hinge giving the Case NN2a, so we can proceed to propogate the arrows upwards along tetrahedra until we come to another hinge, giving Case NH2a, which is then a horizontal reflection of case HN1a.

Hence, both Case HN1a and Case HN2a lead to a propogation of the arrows upwards, with vertical cycles, one along the vertices corresponding to right veering edges, and the other along left veering edges.

Case HN1b leads to an orientation on the non-hinge which is a vertical reflection of the orientation on the non-hinge in Case NN1a, and Case HN2b gives an orientation on the non-hinge (up to vertical reflection) as in the Case NN2a. In this case, the arrows propogate downwards along tetrahedra, again forming vertical cycles.

Hence, regardless of the choice, if r is in the kernel of A^T, we must have that $r_{x_i} = r_{x_j}$ and $r_{y_i} = r_{y_j}$ for all $i \neq j$. Since we know from Proposition 5.9 that the vector $r_c = (1, 1, 1, \ldots, 1)$ is in the kernel of A^T. Let r_x be the vector with ith entry equal to 1 if g_i consists of a product of x's and two z's and 0 otherwise, and let $r_y = r_c - r_x$ be the vector with ith entry equal to 1 if g_i consists of a products of y's and two z's. If any linear combination of r_x and r_y besides a multiple of r_c is in the kernel of A^T, by subtracting an appropriate multiple of r_c and scaling, we would have r_x (and r_y) in the kernel of A^T.

We claim that neither r_x nor r_y are in the kernel of A^T. Take any tetrahedron T_j where y_j has angle π. Then, by construction, the jth row of A^T has negative entry in the ith column when x_j or z_j is in the ith gluing equation. In particular, the jth entry of $A^T r_x$ is $-2c_j + \delta$ where δ is non-positive and is $-(1 - c_j)$ if z_j appears in one of the gluing equations with all x's and $-2(1 - c_j)$ if both z_js appears in gluing equations with x's. Hence, $A^T r_x \neq 0$. Similarly, $A^T r_y \neq 0$, so r_c generates the entire kernel of A^T.

Finally, notice that we have considered inequalities of the type $2r_d \geq 2r_a \geq r_k + r_l$ and $2r_d \leq 2r_a \leq r_k + r_l$ instead of the strict inequalities of Equations 5.3. This reduces the number of base cases, but this means that a particular edge of the monodromy triangulation may have arrows in both directions in the case of equality. However, if at any stage in the induction, we have equality (i.e. an edge has arrows pointing in both directions), then the equalities propogate backwards all the way to the initial hinge, leaving a choice of either $r_{z_i} \geq r_{x_i}$ (or r_{y_i}) or $r_{z_i} \leq r_{x_i}$ (or r_{y_i}) in the forwardmost tetrahedron. A choice of either inequality then continues the induction, giving the same result. □

The previous Proposition establishes smoothness of the tetrahedral variety, using the combinatorics of the cusp. Thus, to show that we can deform the tetrahedra from the real solutions to complex ones, we need only find a vector v in the kernel of A. If v contains all positive entries, then we can deform the shape paremeters of the tetrahedra so that the infinitesimal change in the shape parameters is iv. The imaginary parts of all of the tetrahedra will be positive, and all of the tetrahedra are positively oriented.

Proposition 5.12 (Danciger [6], Proposition 53)**.** *The kernel of A is spanned by a vector with strictly positive entries.*

For the triangulated case, this method gives an alternate, combinatorial proof to

the result of Danciger [6].

Theorem 5.13 (Danciger [6])**.** *Let S be a punctured torus and $\phi : S \to S$ pseudo-Anosov. Then there exists a triangulation of $N_\phi = M_\phi \setminus \Sigma$ and degenerate (real) solutions to the edge consistency equations that can be deformed to a solution with non-degenerate, positive volume tetrahedra.*

5.6 The general case

Although Theorem 5.8 applies to the general case where S is any hyperbolic surface, the argument for the smoothness of the deformation variety for the veering triangulation becomes much more complicated. The inequality in 5.2 can still be used to generate arrows on the triangulation of the cusps, but more cases need to be considered. For example, the inequality

$$r_k + r_l > r_a + r_b$$

means that one of the following hold:

$$r_k > r_a, r_k > r_b$$
$$r_l > r_a, r_l > r_b$$
$$r_k > r_a, r_l > r_a$$
$$r_k > r_b, r_l > r_b.$$

Using these cases, we can attempt to generate directed cycles on the 1-skeleton of the triangulation. However, the number of cases makes it difficult to generalize the argument.

In fact, the volume maximization method to find the complete hyperbolic structure

on the veering triangulation for N_ϕ fails in the general case [19]. However, it is possible that the veering triangulation can be realized geometrically with additional assumptions on ϕ, similar to those used in Theorem 4.5.

5.7 Example: 4-strand braid

We demonstrate the methods established in this chapter on the 4-strand pseudo-Anosov braid with minimal dilatation, $\phi = \sigma_3\sigma_2\sigma_1^{-1}$ as shown by Ko, Los, and Song [26]. The dilatation factor is

$$\lambda_\phi = \frac{1+\sqrt{3}}{2} - \frac{\sqrt[4]{3}}{\sqrt{2}} = 2.29663\ldots,$$

where λ_ϕ satisfies

$$\lambda_\phi^4 - 2\lambda_\phi^3 - 2\lambda_\phi + 1 = 0.$$

The computation of the maximal splitting sequence for this braid is done by Agol [1]. Figure 5.26 shows a train track for the invariant foliation. The 4-braid is viewed as a map on the 5-punctured sphere. In the figure, the four punctures from the strands of the braid are shown, with the fifth puncture being the boundary of a disk containing the figure.

The weights on the train track branches can be retrieved from the maximal splitting sequence or by applying ϕ to the train track in Figure 5.26. In terms of λ_ϕ, the weights for the branches are as follows.

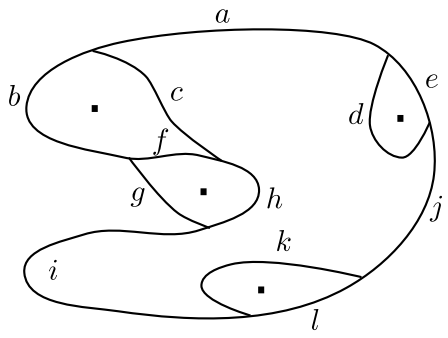

Figure 5.26: A train track for the invariant foliation of $\sigma_3\sigma_2\sigma_1^{-1}$.

$$
\begin{aligned}
a &= -\frac{5}{3}\lambda_\phi^{-3} + 3\lambda_\phi^{-2} + \lambda_\phi^{-1} + \frac{7}{3} = 3.19994\ldots \\
b &= -\frac{4}{3}\lambda_\phi^{-3} + 2\lambda_\phi^{-2} + \lambda_\phi^{-1} + \frac{8}{3} = 3.3712\ldots \\
c &= \frac{1}{3}\lambda_\phi^{-3} - \lambda_\phi^{-2} + \frac{1}{3} = 0.17126\ldots \\
d &= -\frac{2}{3}\lambda_\phi^{-3} + \lambda_\phi^{-2} + \lambda_\phi^{-1} + \frac{1}{3} = 0.90331\ldots \\
e &= -\lambda_\phi^{-3} + 2\lambda_\phi^{-2} + 2 = 2.29663\ldots \\
f &= -\frac{2}{3}\lambda_\phi^{-3} + \lambda_\phi^{-2} + \lambda_\phi^{-1} + \frac{4}{3} = 1.90331\ldots \\
g &= -\frac{2}{3}\lambda_\phi^{-3} + \lambda_\phi^{-2} + \frac{4}{3} = 1.46789\ldots \\
h &= -\frac{1}{3}\lambda_\phi^{-3} + \lambda_\phi^{-1} + \frac{5}{3} = 2.07457\ldots \\
i &= \frac{1}{3}\lambda_\phi^{-3} - \lambda_\phi^{-2} + \lambda_\phi^{-1} + \frac{1}{3} = 0.60668\ldots \\
j &= -\frac{1}{3}\lambda_\phi^{-3} + \lambda_\phi^{-2} - \lambda_\phi^{-1} + \frac{5}{3} = 1.39332\ldots \\
k &= -\frac{1}{3}\lambda_\phi^{-3} + \lambda_\phi^{-2} - \lambda_\phi^{-1} + \frac{2}{3} = 0.39332\ldots \\
l &= 1.
\end{aligned}
$$

Numbering the tetrahedra $T_1, T_2, T_3, T_4, T_5, T_6$ in the order of their dual train track

splits, we have that the edge consistency equations are

$$z_1x_2x_5z_6 = 1 \tag{5.4}$$

$$x_2z_3z_4x_5 = 1 \tag{5.5}$$

$$y_1z_1y_2y_3y_4y_5y_6z_6 = 1 \tag{5.6}$$

$$y_1y_2y_3z_3y_4z_4y_5y_6 = 1 \tag{5.7}$$

$$x_1z_2x_3x_4z_5x_6 = 1 \tag{5.8}$$

$$x_1z_2x_3x_4z_5x_6 = 1. \tag{5.9}$$

The three trivial relations coming from the cusps are

$$\begin{aligned}&(\text{Equation 5.4}) \times (\text{Equation 5.5}) \times (\text{Equation 5.6}) \times (\text{Equation 5.7})\\ &\qquad \times (\text{Equation 5.9}) \times (\text{Equation 5.9}),\\ &(\text{Equation 5.5}) \times (\text{Equation 5.6}) \times (\text{Equation 5.8}),\\ &(\text{Equation 5.4}) \times (\text{Equation 5.7}) \times (\text{Equation 5.8}).\end{aligned}$$

The shape parameters z_i are computed from the cross ratios

$$\begin{aligned}z_1 &= (a, g; b, 0) = 0.041276\ldots\\ z_2 &= (e, g; a, 0) = \frac{1}{3}\\ z_3 &= (a - d - g, d; e, 0) = 1.14832\ldots\\ z_4 &= (f, g; h, 0) = 0.21771\ldots\\ z_5 &= (b - c - g, g; f, 0) = \frac{1}{3}\\ z_6 &= (a - d - g, g; b - c - g, 0) = 6.0568\ldots.\end{aligned}$$

It is easily checked that these shape parameters satisfy the edge consistency equations

5.4–5.9. For this example, the method outline in Section 5.6 works to show smoothness of the deformation variety for the veering triangulation. In fact, numbering the edges 1–6 by the order in which they appear in the edge consistency equations of 5.4–5.9, we can see that Equation 5.2 for T_1 becomes one of either

$$r_1 + r_3 > r_5 + r_6 > r_3 + r_4$$
$$r_3 + r_4 > r_5 + r_6 > r_1 + r_3.$$

Without loss of generality, assume that $r_1+r_3 > r_5+r_6 > r_3+r_4$. Then, the equation from T_2 is forced to be

$$r_5 + r_6 > r_1 + r_2 > r_3 + r_4$$

since $r_5 + r_6 > r_3 + r_4$. We can then proceed to T_3 to find that

$$r_5 + r_6 > r_3 + r_4 > r_2 + r_4.$$

Now, Equation 5.2 on T_4 states that either

$$r_3 + r_4 > r_5 + r_6 > r_2 + r_4$$

or

$$r_2 + r_4 > r_5 + r_6 > r_3 + r_4.$$

But we already have that $r_5 + r_6 > r_3 + r_4$ and $r_5 + r_6 > r_2 + r_4$, so neither can be satisfied by strict inequality. Hence, we have that $r_5+r_6 = r_1+r_2 = r_3+r_4 = r_2+r_4$. Then, $r_1+r_3 = r_5+r_6$ is also forced by T_6. By Proposition 5.10, then the deformation variety is smooth. To find a deformation of the real solutions to positively oriented tetrhedra, we must find a vector ξ satisfying Equation 5.1 with strictly positive entries [6, Theorem 8].

The matrix A has the form

$$A = \begin{bmatrix} -(1-c_1) & 1 & 0 & 0 & 1 & -(1-c_6) \\ 0 & 1 & -(1-c_3) & -(1-c_4) & 1 & 0 \\ -c_1-(1-c_1) & -c_2 & 1 & -c_4 & -c_5 & 1-(1-c_6) \\ -c_1 & -c_2 & 1-(1-c_3) & -c_4-(1-c_4) & -c_5 & 1 \\ 1 & -(1-c_2) & -c_3 & 1 & -(1-c_5) & -c_6 \\ 1 & -(1-c_2) & -c_3 & 1 & -(1-c_5) & -c_6 \end{bmatrix},$$

where

$$\begin{aligned} c_1 &= z_1 \\ c_2 &= z_2 \\ c_3 &= \frac{1}{z_3} \\ c_4 &= z_4 \\ c_5 &= z_5 \\ c_6 &= \frac{1}{z_3}. \end{aligned}$$

The kernel has dimension $\dim \ker A = 3$ and is spanned by

$$v_1 = \begin{pmatrix} -5.38748\ldots \\ -4.33021\ldots \\ -6.49531\ldots \\ 0 \\ 0 \\ 1 \end{pmatrix}$$

$$v_2 = \begin{pmatrix} 0.504107\ldots \\ -0.5167\ldots \\ 0.72495\ldots \\ 0 \\ 1 \\ 0 \end{pmatrix}$$

$$v_3 = \begin{pmatrix} 4.64148\ldots \\ 4.4499\ldots \\ 6.48111\ldots \\ 1 \\ 0 \\ 0 \end{pmatrix}.$$

The vector $v = v_1 + v_2 + 2v_3$ has all positive entries, so we can find a deformation of the real shape parameters (z_j) in the direction of iv, so that the tetrahedra become positively oriented with positive volume.

Bibliography

[1] Ian Agol, *Ideal triangulations of pseudo-Anosov mapping tori*, Topology and geometry in dimension three, Contemp. Math., vol. 560, Amer. Math. Soc., Providence, RI, 2011, pp. 1–17. MR 2866919 (2012m:57026)

[2] Ian Agol, Daniel Groves, and Jason Manning, *The virtual Haken conjecture*, arXiv:1205.0825 (2010).

[3] Francis Bonahon, *Geometric structures on 3-manifolds*, Handbook of Geometric Topology (R.B. Sher and R.J. Daverman, eds.), Elsevier, 2002, pp. 93–164.

[4] Young-Eun Choi, *Positively oriented ideal triangulations on hyperbolic three-manifolds*, Topology **43** (2004), no. 6, 1345–1371. MR 2081429 (2005i:57016)

[5] Daryl Cooper and Bill Goldman, *A 3-manifold with no real projective structure*, arXiv:1207.2007 (2012).

[6] Jeffrey Danciger, *Geometric transitions: from hyperbolic to ads geometry*, Stanford University Thesis (2011).

[7] Charles Ehresmann, *Sur les espaces localement homogenes*, L'Enseignement Mathmatique **35** (1936), 317–333.

[8] D. B. A. Epstein and R. C. Penner, *Euclidean decompositions of noncompact hyperbolic manifolds*, J. Differential Geom. **27** (1988), no. 1, 67–80. MR 918457 (89a:57020)

[9] Benson Farb and Dan Margalit, *A primer on mapping class groups*, Princeton University Press, 2011.

[10] David Futer and François Guéritaud, *Explicit angle structures for veering triangulations*, Algebr. Geom. Topol. **13** (2013), no. 1, 205–235. MR 3031641

[11] William M. Goldman, *Geometric structures on manifolds and varieties of representations*, Geometry of group representations (Boulder, CO, 1987), Contemp. Math., vol. 74, Amer. Math. Soc., Providence, RI, 1988, pp. 169–198. MR 957518 (90i:57024)

[12] François Guéritaud, *On canonical triangulations of once-punctured torus bundles and two-bridge link complements*, Geom. Topol. **10** (2006), 1239–1284, With an appendix by David Futer. MR 2255497 (2007g:57009)

[13] Michael Heusener, Joan Porti, and Eva Suárez, *Regenerating singular hyperbolic structures from Sol*, J. Differential Geom. **59** (2001), no. 3, 439–478. MR 1916952 (2003e:57026)

[14] Michael Heusener, Joan Porti, and Eva Suárez Peiró, *Deformations of reducible representations of 3-manifold groups into* $\mathrm{SL}_2(\mathbf{C})$, J. Reine Angew. Math. **530** (2001), 191–227. MR 1807271 (2002a:57002)

[15] Craig Hodgson, *Degeneration and regeneration of geometric structures on 3-manifolds*, Ph.D. thesis (1986).

[16] Craig D. Hodgson and Steven P. Kerckhoff, *Rigidity of hyperbolic cone-manifolds and hyperbolic Dehn surgery*, J. Differential Geom. **48** (1998), no. 1, 1–59. MR 1622600 (99b:57030)

[17] ———, *Universal bounds for hyperbolic Dehn surgery*, Ann. of Math. (2) **162** (2005), no. 1, 367–421. MR 2178964 (2006g:57031)

[18] Craig D. Hodgson, J. Hyam Rubinstein, Henry Segerman, and Stephan Tillmann, *Veering triangulations admit strict angle structures*, Geom. Topol. **15** (2011), no. 4, 2073–2089. MR 2860987

[19] Ahmad Issa, Personal communication, 2012.

[20] Silvio Levy (ed.), *Three-dimensional geometry and topology*, vol. 1, Princeton University Press, 1997.

[21] Joseph Maher, *Random walks on the mapping class group*, Duke Math. J. **156** (2011), no. 3, 429–468. MR 2772067 (2012j:37069)

[22] Curtis T. McMullen, *Billiards and Teichmüller curves on Hilbert modular surfaces*, J. Amer. Math. Soc. **16** (2003), no. 4, 857–885 (electronic). MR 1992827 (2004f:32015)

[23] R.C. Penner and J.L. Harer, *Combinatorics of train tracks*, Princeton University Press, 1992.

[24] Joan Porti, *Torsion de Reidemeister pour les variétés hyperboliques*, Mem. Amer. Math. Soc. **128** (1997), no. 612, x+139. MR 1396960 (98g:57034)

[25] Igor Rivin, *Walks on groups, counting reducible matrices, polynomials, and surface and free group automorphisms*, Duke Math. J. **142** (2008), no. 2, 353–379. MR 2401624 (2009m:20077)

[26] Won Taek Song, Ki Hyoung Ko, and Jérôme E. Los, *Entropies of braids*, J. Knot Theory Ramifications **11** (2002), no. 4, 647–666, Knots 2000 Korea, Vol. 2 (Yongpyong). MR 1915500 (2003e:57013)

[27] William P. Thurston, *The geometry and topology of three-manifolds*, http://www.msri.org/publications/books/gt3m/, 1980.

[28] ———, *On the geometry and dynamics of diffeomorphisms of surfaces*, Bull. Amer. Math. Soc. (N.S.) **19** (1988), no. 2, 417–431. MR 956596 (89k:57023)

[29] ———, *Hyperbolic structures on 3-manifolds, ii: Surface groups and 3-manifolds which fiber over the circle*, arXiv:math/9801045 (1998).